DOI: 10.1002/chem.200600110

Ruthenation of Duplex and Single-Stranded d(CGGCCG) by Organometallic Anticancer Complexes

Hong-Ke Liu,[a, c] Fuyi Wang,[a] John A. Parkinson,[b] Juraj Bella,[a] and Peter J. Sadler*[a]

Abstract: We have studied the interaction of the organometallic anticancer ruthenium(II) complexes [(η^6-*p*-cymene)Ru(en)Cl][PF_6] (**1**) and [(η^6-biphenyl)Ru(en)Cl][PF_6] (**2**) (en = ethylenediamine) with the single-stranded (ss) DNA hexamer d(CGGCCG) (**I**) and the duplex d(CGGCCG)$_2$ (**II**) by HPLC, ESI-MS, and one- and two-dimensional ^{1}H and ^{15}N NMR spectroscopy. For ss-DNA, all three G's are readily ruthenated with [(η^6-arene)-Ru(en)]$^{2+}$, but for duplex DNA there is preferential ruthenation of G3 and G6, and no binding to G2 was detected. For monoruthenated duplexes, N7 ruthenation of G is accompanied by strong hydrogen bonding between G-O6 and en-N*H* for the *p*-cymene adducts. Intercalation of the non-coordinated phenyl ring between G3 and C4 or G6 and C5 was detected in the biphenyl adducts of mono- and diruthenated duplexes, together with weakening of the G-O6···N*H*-en hydrogen bonding. The arene ligand plays a major role in distorting the duplex either through steric interactions (*p*-cymene) or through intercalation (biphenyl).

Keywords: antitumor agents · arenes · DNA · intercalation · NMR spectroscopy · ruthenium

Introduction

Organometallic ruthenium(II)–arene complexes of the type [(η^6-arene)Ru(XY)Cl]$^+$ (e.g., arene = biphenyl, XY = ethylenediamine (en)) exhibit anticancer activity both in vitro and in vivo.[1-4] These complexes are monofunctional; that is, they have one reactive chloride ligand that can undergo activation through aquation and bind strongly to N7 of G on DNA.[5–7] The widely used anticancer drug cisplatin is also activated through aquation, but is bifunctional and can bind to two neighbouring guanines on DNA, causing the double helix to bend.[8] In work on adducts of [(η^6-arene)Ru(XY)Cl]$^+$ with guanosine and guanosine 5′-monophosphate, we found that binding of Ru to G-N7 can be accompanied by strong hydrogen bonding between G-O6 and en-N*H*, together with π–π stacking between the purine ring of G and the arene when the arene is extended (e.g. arene = biphenyl or tetrahydroanthracene).[6]

The aim of the present work was to investigate the interaction of these ruthenium–arene anticancer complexes with single-strand and duplex DNA. We chose the short self-complementary hexamer d(CGGCCG), because it is known to crystallise readily and can accommodate organic intercalators.[9] We have compared reactions of two ruthenium–arene complexes [(η^6-arene)Ru(en)Cl]$^+$, arene = *p*-cymene (complex **1**) and biphenyl (complex **2**), with the DNA single strand d(CGGCCG) and the DNA duplex d(CGGCCG)$_2$. The arenes were chosen as examples of potential intercalators (biphenyl) and nonintercalators (*p*-cymene). Unfortunately, crystals of the ruthenated duplex grown by vapour diffusion from sitting drops diffracted X-rays too poorly to allow a structure determination.[10] Therefore in this work, we have used NMR spectroscopy to obtain structural information in solution. We have compared the ruthenation of duplex DNA with that of the single strands. This has revealed some interesting features of the specificity of ruthenation. Solution studies on this DNA are complicated by the presence of three potential ruthenation sites on each strand, but HPLC has allowed us to separate and identify the sites

[a] Dr. H.-K. Liu, Dr. F. Wang, J. Bella, Prof. P. J. Sadler
School of Chemistry, University of Edinburgh
King's Buildings, West Mains Road, Edinburgh EH9 3 JJ (UK)
Fax: (+44) 131-650-6453
E-mail: P.J.Sadler@ed.ac.uk

[b] Dr. J. A. Parkinson
WestCHEM, Department of Pure and Applied Chemistry
University of Strathclyde, Thomas Graham Building
295 Cathedral Street, Glasgow G1 1XL (UK)

[c] Dr. H.-K. Liu
Current address:
School of Chemistry and Environmental Science
Nanjing Normal University, Nanjing 210046 (P.R. China)

Supporting information for this article is available on the WWW under http://www.chemeurj.org/ or from the author.

of ruthenation, which has simplified interpretation of the NMR spectra.

Results

We studied reactions of the *p*-cymene complex **1** and biphenyl complex **2** with the self-complementary DNA hexamer d(CGGCCG) (Figure 1) at low ionic strength in which

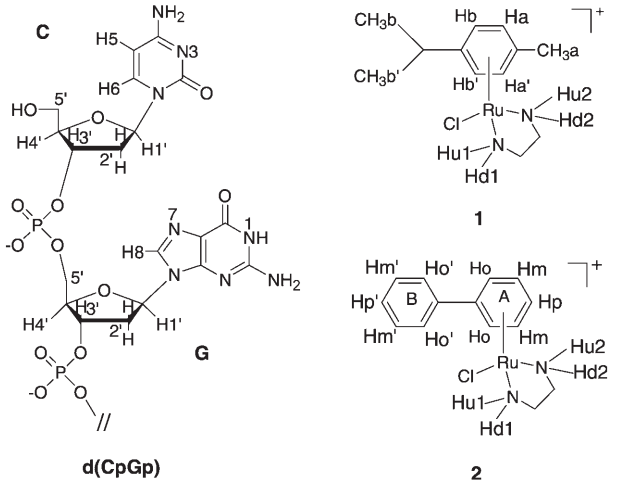

Figure 1. Structures and NMR numbering schemes for the cations of [(η^6-*p*-cymene)Ru(en)Cl][PF_6] (**1**) and [(η^6-biphenyl)Ru(en)Cl][PF_6] (**2**), and for the 5′-d(CpGp) fragment of the hexamer d(CGGCCG); en = ethylenediamine.

it is largely a single strand (**I**) and at high ionic strength (100 mM $NaClO_4$, I = 0.05) in which it is largely a duplex (**II**), at molar Ru/**I** and Ru/**II** ratios of 0.5–6.0:1.0 and 1.0:1.0, respectively. These reactions proceed through hydrolysis of the chloro complex to give the aqua adducts [(η^6-arene)Ru(en)(H_2O)]$^{2+}$, which are more reactive towards DNA bases.[7] We used reverse-phase HPLC to separate equilibrium mixtures, mass spectrometry to identify the products and NMR spectroscopy to determine the ruthenation sites.

Scheme 1 indicates the reaction pathways that were followed during the course of this study. HPLC led to the separation of single strands, even for reactions of the duplex. Four equilibrium mixtures resulting from reactions shown in Scheme 1 (**II**+**1**, **II**+**2**, **I**+**1** and **I**+**2**) and a diruthenated duplex (**II**–Ru_2–G3G9, formed by annealing HPLC-separated fractions **I**–Ru–G3 (Ru = [(η^6-biphenyl)Ru(en)]$^{2+}$, Scheme 1) were studied by one-dimensional ^{1}H, ^{15}N-decoupled two-dimensional [^{1}H,^{1}H] COSY, TOCSY, ROESY, NOESY and ^{15}N-decoupled two-dimensional [^{1}H,^{15}N] HSQC NMR experiments by using ^{15}N-en labelled complexes. Although the equilibrium reaction mixtures gave complicated NMR spectra, it was possible to make complete assignments of proton resonances for the ruthenated species present with

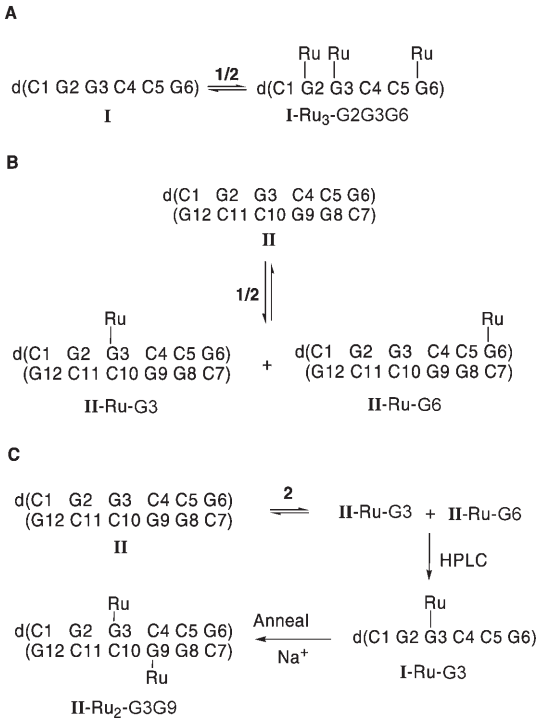

Scheme 1. A) Reaction of single-stranded (ss) hexamer **I** (0.2 mM) with 3–6 mol equiv of **1** or **2** in 90% H_2O/10% D_2O, 310 K for 48 h, gives triruthenated **I** (**I**–Ru_3–G2G3G6). B) Reaction of double-stranded (ds) hexamer **II** (0.3 mM, 0.1 M $NaClO_4$) with 1 mol equiv of **1** or **2** in 90% H_2O/10% D_2O gives rise to two monoruthenated duplexes **II**–Ru–G3 and **II**–Ru–G6 as products. C) Reaction of duplex **II** (0.3 mM, 0.1 M $NaClO_4$) with 1 mol equiv of **2** gives two main products: **II**–Ru–G3 and **II**–Ru–G6. After HPLC separation, the monoruthenated single-stranded **I**–Ru–G3 was collected, and annealed to form the diruthenated product **II**–Ru_2–G3G9. Ru = bound fragments [(η^6-*p*-cymene)Ru(en)]$^{2+}$ (**1′**) or [(η^6-biphenyl)Ru(en)]$^{2+}$ (**2′**); for structures of **1** and **2**, see Figure 1.

the aid of the HPLC and MS data. This procedure allowed us to investigate the sequence specificity of ruthenation of guanine residues in the context of CpG, GpG and GpC base steps and also to compare the structural perturbations induced by *p*-cymene and biphenyl arenes.

HPLC and ESI-MS characterisation of products

*ss-DNA **I**+*p*-cymene complex **1** or biphenyl complex **2***: Aqueous solutions of **1** or **2** were incubated with **I** at 310 K at Ru/**I** molar ratios ranging from 0.5:1 to 6.0:1 for 48 h, and were then analysed by HPLC. New peaks were observed for each reaction (Figure 2), and the adducts associated with them were identified subsequently by ESI-MS. The peaks for the observed negative ions are shown in Figure S1 and listed in Table S1 in the Supporting Information. Reaction at a Ru/**I** molar ratio of 0.5:1 resulted in three monoruthenated products, and at a 1:1 molar ratio the same three monoruthenated products together with three diruthenated products. Reaction at a Ru/**I** molar ratio of 6:1 (for **1**) or 3:1 (for **2**), gave only one main HPLC peak corresponding to a triruthenated product.

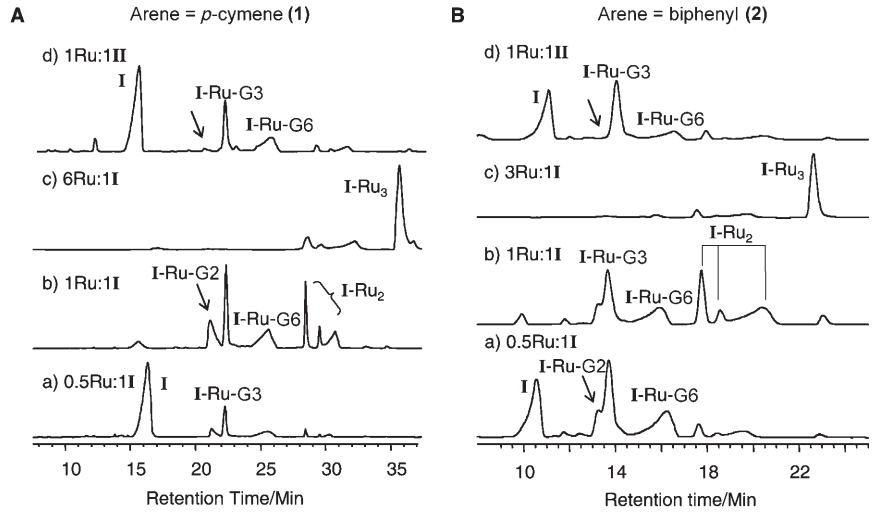

Figure 2. HPLC data for reaction of $[(\eta^6\text{-}p\text{-cymene})RuCl(en)]PF_6$ (**1**) (panel A) or $[(\eta^6\text{-biphenyl})RuCl(en)]PF_6$ (**2**) (panel B) with ss-DNA d(CGGCCG) (**I**) (0.1 mM in H_2O) at Ru/**I** mol ratios of a) 1:2, b) 1:1, c) 6:1 (for **1**) or 3:1 (for **2**), and d) for reaction of **1** or **2** with ds-DNA $d(CGGCCG)_2$ (**II**) (0.3 mM, 0.1 M $NaClO_4$, 90% H_2O/10% D_2O) at a Ru/**II** mol ratio of 1:1. The monoruthenated duplex **II**–Ru_1 elutes as monoruthenated ss-DNA **I** (**I**–Ru–G3 and **I**–Ru–G6, see d). It is notable that G2 is readily ruthenated for single strand **I** (see **I**–Ru–G2 in a) but not for duplex **II** (see d). Ru = $[(\eta^6\text{-}p\text{-cymene})Ru(en)]^{2+}$ (**1′**) or $[(\eta^6\text{-biphenyl})Ru(en)]^{2+}$ (**2′**), and is bound to G3N7 or G6N7; for DNA sequence, see Scheme 1.

*Duplex **II**+**1** or **2***: An aqueous solution of **1** or **2** was incubated with duplex **II** in 0.1 M $NaClO_4$ at ambient temperature for three weeks (for **1**) or two days (for **2**) at a Ru/**II** molar ratio of 1:1. The equilibrium mixtures gave HPLC peaks that were identified by ESI-MS as ss-DNA **I** and two monoruthenated single-strand products (see Figure 2d, Figure S1, and Table S1 in the Supporting Information), with relative peak area ratios of 1.2:1 (for **II**+**1**) and 3:1 (for **II**+**2**). The HPLC peak for the major monoruthenated single-strand adduct in the 1:1 equilibrium mixture of **II**+**2** was collected, desalted and annealed by adding 100 mM $NaClO_4$ to give the diruthenated duplex **II**–Ru_2–G3G9 (see Scheme 1C). The melting temperature (T_m) of this diruthenated duplex was 302.3 ± 0.9 K (100 mM $NaClO_4$), which is 14 K lower than that of the free duplex **II** ($T_m = 316.8 \pm 0.1$ K).

NMR characterisation of products: The assignments of the ^{1}H NMR resonances of free DNA duplex **II** have been reported by Lam and Au-Yeung[11] and the chemical shifts are listed in Table S3 in the Supporting Information. Assignments of the ^{1}H NMR peaks for the ruthenated DNA duplexes were made on the basis of the established methods developed for studying right-handed B-DNA duplexes by NMR spectroscopy.[12–15] Terminal (3′) base resonance assignments were identified from NOESY NMR data sets and were based on ordering of the H2′ and H2″ proton chemical shifts (δH2′ > δH2″) compared with the other nucleotide units (δH2′ < δH2″).

II*+p-*cymene complex* *1: Figure 3 shows the imino and aromatic region of the 600 MHz ^{1}H NMR spectrum of DNA duplex **II** in the absence (Figure 3A) and presence (Figure 3B) of one molar equivalent of **1**. The binding of **1** resulted in the formation of a number of new peaks (especially near 8.5 ppm), and the broadening of many DNA proton resonances. It is notable that after ruthenation, the intensity of the DNA imino proton resonances for the terminal base-pairs G6·C7 and G12·C1 increased ($\delta = 13.19$ ppm). Two imino proton resonances were shifted to high field by 0.19 (G3*) and 0.11 ppm (G6*), respectively, relative to duplex **II** (Figure 3, Tables 1 and 2).

Two major new species were detected by two-dimensional [^{1}H,^{15}N] HSQC NMR analysis of the equilibrium mixture of duplex **II** and ^{15}N-**1** (the ^{15}N labelled *p*-cymene complex **1**) at 283 K in 90% H_2O/10% D_2O (Figure 4A) or D_2O (Figure 4B) by analysis of peaks assignable to en-NHu resonances (the NH protons oriented towards the coordinated arene ring, see Figure 1 and Table S2 in the Supporting Informa-

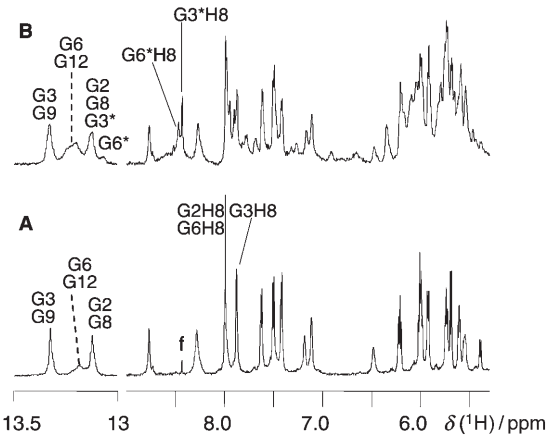

Figure 3. 600-MHz ^{1}H NMR spectra of the imino and aromatic region for A) duplex $d(CGGCCG)_2$ (**II**) and B) the 1:1 equilibrium mixture of duplex **II** and complex **1** in 90% H_2O/10% D_2O at 283 K, 0.1 M $NaClO_4$ at pH 7.0. Assignments of DNA imino resonances (13–13.5 ppm) and G-H8 resonances (ca. 8.0 ppm) are indicated and resonances for ruthenated guanines are marked with asterisks. Broadening of resonances and the appearance of new peaks in B are due to the ruthenation of duplex **II**. The increase in the intensity of the imino peaks for the terminal bases G6 and G12 when the duplex is ruthenated suggests an increase in imino proton residence time within terminal base-pairs indicative of base-pair stabilisation in what are normally regarded as "frayed ends". The assignments of peaks G3* and G6* to two monoruthenated duplexes are based on two-dimensional correlation experiments (shown in Figure 5, see also Tables 1–3); f = formate impurity.

Table 1. ^{1}H NMR chemical shifts for the product Ru–**II**a in the 1:1 equilibrium mixture of duplex **II** and complex **1** (283 K; Ru = [(η^6-*p*-cymene)Ru(en)]$^{2+}$).

Residue[a]	Proton[b]								
	H8	H6	H5	H1′	H2′	H2″	H3′	H4′	imino
C1		7.66	5.95	5.76	1.93	2.40	4.75	4.09	
G2	7.96			5.56	2.77	2.77	5.04	4.34	13.15
G3	8.48			6.36	2.79	2.92	5.03	n.a.[d]	13.16
	(0.58)[c]			(0.33)	(0.09)	(0.13)			(−0.19)
C4		7.85	6.09	6.09	2.12	2.50	4.85	n.a.	
		(0.40)	(0.67)	(0.06)					
C5		7.51	5.81	5.62	2.04	2.36	4.90	4.14	
			(0.09)						
G6	8.00			6.22	2.67	2.40	4.75	4.24	13.21
C7		7.66	5.95	5.76	1.93	2.40	4.75	4.09	
G8	7.96			5.56	2.77	2.77	5.04	4.34	13.15
G9	7.90			6.02	2.70	2.77	5.07	4.46	13.35
C10		7.52	5.56	6.13	2.14	2.54	4.90	n.a.	
		(0.07)	(0.14)	(0.10)		(0.05)			
C11		7.54	5.73	5.62	2.04	2.36	4.88	4.14	
G12	8.00			6.22	2.67	2.40	4.75	4.24	13.21

[a] For DNA sequence, see Scheme 1. [b] For atom labels, see Figure 1. [c] Values in brackets are chemical shift changes from free **II** (see Table S3 in the Supporting Information) of $\geq$0.05 ppm [$\Delta\delta = \delta$(Ru–**II**a)$-\delta$(**II**)]. [d] n.a. = not assigned. **1**′ is bound at N7 of G3.

Table 2. ^{1}H NMR chemical shifts for product Ru–**II**b in the 1:1 equilibrium mixture of duplex **II** and complex **1** (283 K; Ru = [(η^6-*p*-cymene)Ru(en)]$^{2+}$).

Residue[a]	Proton[b]								
	H8	H6	H5	H1′	H2′	H2″	H3′	H4′	imino
C1		7.66	5.95	5.76	1.93	2.40	4.75	4.09	
G2	7.96			5.56	2.77	2.77	5.04	4.34	13.15
G3	7.89			6.01	2.70	2.77	5.07	n.a.[c]	13.35
C4		7.48	5.51	6.02	2.09	2.48	4.90	4.24	
C5		7.94	6.11	6.11	2.12	2.50	n.a.	n.a.	
		(0.41)[d]	(0.39)	(0.46)	(0.05)	(0.11)			
G6	8.51			6.36	2.98	2.54	4.75	n.a.	13.10
	(0.49)			(0.12)	(0.28)	(0.12)			(−0.11)
C7		7.72	5.84	5.95	1.93	2.43	n.a.	4.10	
		(0.06)	(−0.12)	(0.17)					
G8	7.96			5.56	2.77	2.77	5.04	4.34	13.15
G9	7.90			6.02	2.70	2.77	5.07	4.46	13.35
C10		7.48	5.47	6.02	2.09	2.48	4.90	4.24	
C11		7.54	5.73	5.62	2.04	2.36	4.88	4.14	
G12	8.00			6.22	2.67	2.40	4.75	4.24	13.21

[a] For DNA sequence, see Scheme 1. [b] For atom labels, see Figure 1. [c] n.a. = not assigned. [d] Values in brackets are chemical shift changes from free **II** (see Table S3 in the Supporting Information) of $\geq$0.05 ppm [$\Delta\delta = \delta$(Ru–**II**b)$-\delta$(**II**)]. **1**′ is bound at N7 of G6.

tion) of monoruthenated duplexes Ru–**II**a and Ru–**II**b (Ru = [(η^6-*p*-cymene)Ru(en)]$^{2+}$ (**1**′)). This result is consistent with the HPLC and MS data. Strong cross-peaks for en-NHu resonances of Ru–**II**a and Ru–**II**b (Figure 4B) were still detected after the equilibrium mixture had been freeze-dried, re-dissolved in D_2O and left to stand for 72 h at 283 K. The en-NHd resonances of both Ru–**II**a and Ru–**II**b were not observed. In contrast, the en-NHu and en-NHd resonances of unreacted **1** (and its aqua adducts) were detected in 90% H_2O (Figure 4A), but not in D_2O due to H-D exchange (Figure 4B). The assignments are listed in Table S2 in the Supporting Information.

The two-dimensional [^{1}H,^{1}H] COSY NMR spectrum of the equilibrium mixture of duplex **II** and complex **1** clearly showed the existence of two monoruthenated duplexes Ru–**II**a and Ru–**II**b, as well as unreacted duplex **II**. This can be seen for example in the cytosine H5-H6 cross-peak region shown in Figure 5. Three sets of H5-H6 cross-peaks were detected for the cytosine C4, C5, C7 and C10 residues. The proportions of Ru–**II**a, Ru–**II**b and unreacted duplex **II** were established by integration of the COSY cross-peaks for C4-H5 and C4-H6 of Ru–**II**a, C5-H5 and C5-H6 of Ru–**II**b, and by comparing the HPLC peak areas **I**–Ru–G3:**I**–Ru–G6 from the equilibrium mixture (see Figure 2A, spectrum d). The amounts of free **1** and its aqua adduct H_2O-**1** in the mixture were taken into account. The ratios of Ru–**II**a/Ru–**II**b/duplex **II** were 0.4:0.4:0.2 (±10%). The presence of other complexes was estimated to account for less than 10% of the total duplex.

Assignments for ^{1}H NMR peaks of monoruthenated duplexes Ru–**II**a and Ru–**II**b in the mixture (**II**+**1**) are listed in Tables 1 and 2, and intermolecular NOEs in Table 3. For Ru–**II**a, a large low-field shift of the G3-H8 resonance, relative to free duplex **II**, was observed ($\Delta\delta = 0.58$ ppm), as was also the case for H5 and H6 of the neighbouring C4 base ($\Delta\delta =$ 0.40 and 0.67 ppm, respectively), and H5 of C10 ($\Delta\delta =$ 0.14 ppm) in the second strand, which is paired with G3 (Table S3 in the Supporting Information). The largest changes in deoxyribose H1′ chemical shifts occur for the G3 residue ($\Delta\delta = 0.33$ ppm), with smaller change for the neighbouring C4 ($\Delta\delta = 0.06$ ppm) and C10 ($\Delta\delta = 0.10$ ppm) residues (Figure S2 in the Supporting Information and Table 1). Weak NOE cross-peaks are found between G3-H8 and **1**′-en-N*Hu*, G3-H8 and **1**′-CH_3a, G3-H2″ and **1**′-Hb/**1**′-Hb′ protons, and intermediate intensity cross-peaks between G3-H2′ and **1**′-Hb/**1**′-Hb′, and between G3-H1′ and **1**′-CH protons (Figure 6 and Table 3; for atom labelling see Figure 1).

For the adduct Ru–**II**b large low-field shifts were observed for the G6-H8 resonance ($\Delta\delta = 0.49$ ppm) and for H5 and H6 resonances of the neighbouring C5 residue ($\Delta\delta =$

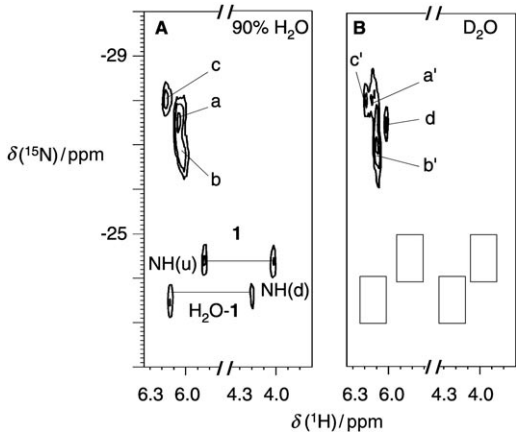

Figure 4. Two-dimensional [^{1}H,^{15}N] HSQC NMR spectra of a 1:1 equilibrium mixture of duplex **II** and ^{15}N-**1** (0.3 mM, 0.1 M $NaClO_4$ at 283 K, pH 7.0) in (A) 90% H_2O/10% D_2O and (B) 100% D_2O after 72 h. Assignments for both en-NH(d) and NH(u) resonances of the unreacted ^{15}N-**1** (aqua species H_2O-**1** and chloro complex **1**) are shown in A); in contrast in B) all NH groups are deuterated for H_2O-**1** and **1** (empty boxes in B). Assignments: a, a′ = en-NH(u) resonances of **II**–Ru–G3; b, b′ = en NH(u) resonances of **II**–Ru–G6; c, c′ and d are not assigned. The en NH(d) resonances of both **II**–Ru–G3 and **II**–Ru–G6 were not observed. Strong NH peaks for the DNA-bound complexes were still detected at about 6 ppm for the D_2O solution after 72 h (B), suggesting the existence of strong G-O6···HN-en hydrogen bonding. Ru = [(η^6-*p*-cymene)Ru(en)]$^{2+}$. For atom labels and structures of **II**–Ru–G3 and **II**–Ru–G6, see Figure 1 and Scheme 1.

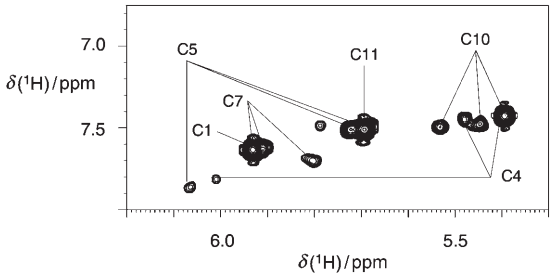

Figure 5. Two-dimensional [^{1}H,^{1}H] COSY NMR spectrum in the cytosine H5/H6 cross-peak region for a 1:1 equilibrium mixture of duplex **II** and **1** (0.3 mM, 0.1 M $NaClO_4$) in 90% H_2O/10% D_2O at 283 K. Note that three sets of resonances are observed for the C4, C5, C7 and C10 residues, suggesting the presence of two monoruthenated products as well as unreacted duplex **II**. Assignments are based on the two-dimensional [^{1}H,^{1}H] NOESY NMR spectrum (see Figure 6 and Tables 1–3); for DNA sequence, see Scheme 1.

0.41, 0.39 ppm, respectively). The H6 resonance of C7 in the complementary strand, which is paired with G6, shifted slightly to low field ($\Delta\delta = 0.06$), but the H5 resonance shifted to high field ($\Delta\delta = -0.12$ ppm) relative to free duplex **II** (Table 2 and Table S3 in the Supporting Information). The largest changes in H1′ chemical shifts were found for C5 ($\Delta\delta = 0.46$ ppm), G6 ($\Delta\delta = 0.12$ ppm) and C7 ($\Delta\delta = 0.17$ ppm) (Figure S2 in the Supporting Information and Table 2). Weak NOE cross-peaks were found between G6-H8 and **1**′-en-NHu, G6-H8 and **1**′-CH_3a, and G6-H1′ and **1**′-CH protons (Figure 6 and Table 3).

Table 3. ^{1}H NMR chemical shifts for [(η^6-*p*-cymene)Ru(en)(Cl)][PF_6] (**1**) and bound fragment [(η^6-*p*-cymene)Ru(en)]$^{2+}$ (**1**′), and intermolecular NOEs in the 1:1 equilibrium mixture of duplex **II** and **1** (at 283 K).

Proton[a]	**1**	**1**′	$\Delta\delta$[b]	NOEs (**II**-**1**′)[e]	
				Ru–**II**a	Ru–**II**b
CH_3a	2.26	1.99	−0.27	G3*H8(w)[c]	G6*H8(w)
CH_3b	1.30	1.13	−0.17		
en-CH_2	2.45	2.51	0.06		
CH	2.86	2.54	−0.32	G3*H1′ (m)	G6*H1′ (m)
en-NHd	4.22	n.a.[d]			
Ha, Ha′	5.60	5.64			
Hb, Hb′	5.81	5.77		G3*H2′ (m)	
				G3*H2″ (w)	
en-NHu	6.15	6.08	−0.07	G3*H8 (w)	G6*H8 (w)

[a] For atom labels and DNA sequence, see Figure 1 and Scheme 1. [b] $\Delta\delta = \delta(\mathbf{1}') - \delta(\mathbf{1})$ (≥ 0.05 ppm). [c] s = strong, m = medium, w = weak. [d] n.a. = not assigned. [e] **1**′ is bound at G3N7 (in Ru-**II**a) or G6N7 (in Ru-**II**b) and ruthenated guanines are marked with asterisks.

Only one set of signals was observed for bound fragment [(η^6-*p*-cymene)Ru(en)]$^{2+}$ (**1**′) in the two ruthenated duplexes Ru–**II**a and Ru–**II**b (Figure S3 and S4 in the Supporting Information and Table 3). Relative to the signals observed for unbound **1**, peaks for **1**′-CH_3a, **1**′-CH_3b and **1**′-CH of the coordinated arene were shifted to high field by 0.27, 0.17 and 0.32 ppm, respectively.

II + *biphenyl complex* ***2***: Comparison of the imino and aromatic regions of the ^{1}H NMR spectrum of duplex **II** in the absence (Figure S5A in the Supporting Information) and in the presence (Figure S5B) of one molar equivalent of complex **2** showed that new peaks appeared, although the imino proton resonances broadened after ruthenation.

Two major new species were detected in the two-dimensional [^{1}H,^{15}N] HSQC NMR spectrum of the 1:1 equilibrium mixture of duplex **II** and ^{15}N-**2** (^{15}N-labelled complex **2**) at 283 K in 90% H_2O/10% D_2O (Figure 7A) or in D_2O (Figure 7B), with peaks assignable to en-NHu and en-NHd (see Figure 1) of Ru–**II**c and Ru–**II**d (Ru = [(η^6-biphenyl)Ru(en)]$^{2+}$ (**2**′)) (for chemical shifts see Table S2 in the Supporting Information). This result is consistent with the HPLC and MS data (Figure 2 and Table S1 in the Supporting Information). Cross-peaks for en-NHu resonances of Ru–**II**c and Ru–**II**d were still detected after the mixture had been freeze-dried and re-dissolved in D_2O and left standing at 283 K for 5 h. The en-NHd resonances of both Ru–**II**c and Ru–**II**d were not observed in D_2O (Figure 7B).

The two-dimensional TOCSY NMR spectrum of the 1:1 equilibrium mixture (**II** + **2**) clearly shows the existence of two monoruthenated duplexes, as seen for example in the aromatic region in Figure 8. Two sets of H5-H6 cross-peaks were detected for the C4, C5, C7 and C10 residues. The proportions of Ru–**II**c and Ru–**II**d at 283 K were determined by integration of the TOCSY cross-peak volumes of C4-H5/C4-H6 of Ru–**II**c, and C5-H5/C5-H6 of Ru–**II**d, and the HPLC peak areas for **I**–Ru–G3 and **I**–Ru–G6 (see Figure 2B, spectrum d). This gave a Ru–**II**c/Ru–**II**d ratio of 3:1 (±10%). Other species account for less than 10% of the total DNA.

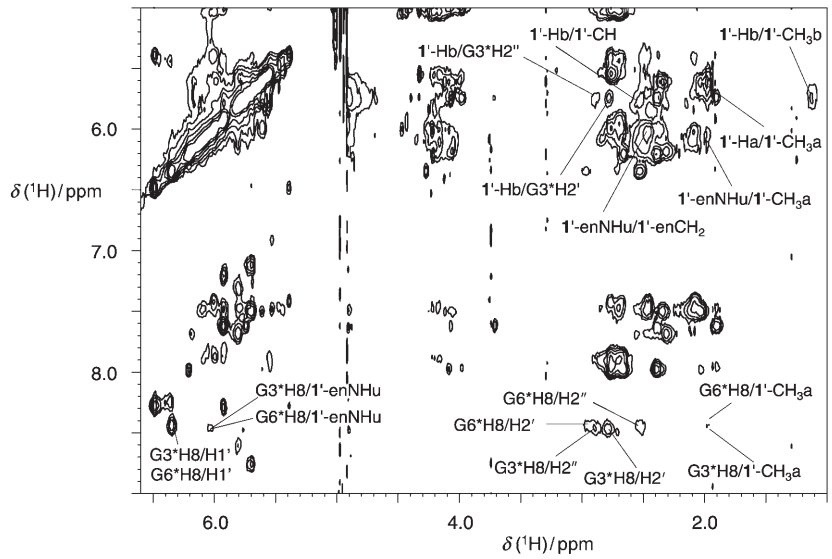

Figure 6. Part of the two-dimensional [^{1}H,^{1}H] NOESY NMR spectrum of the 1:1 equilibrium mixture of duplex **II** and complex **1** (0.3 mM, 0.1 M $NaClO_4$, 90 % H_2O/10 % D_2O at 283 K, pH 7.0, mixing time 400 ms). The observed intermolecular [(η^6-*p*-cymene)Ru(en)]$^{2+}$–**II** cross-peaks from monoruthenated product **II**–Ru–G3 are: G3*H8/**1**′-enNHu, G3*H8/**1**′-CH_3a, **1**′-Hb/G3*H2′ and **1**′-Hb/G3*H2″; and from **II**–Ru–G6 are: G6*H8/**1**′-enNHu and G6*H8/**1**′-CH_3a. Cross-peaks within the ruthenated guanine residues G3* or G6*, and within the bound ruthenium complex **1**′ are also indicated. Labels: **1**′ = [(η^6-*p*-cymene)Ru(en)]$^{2+}$; ruthenated guanines are marked with asterisks. For NMR chemical shifts, see Tables 1–3, and for atom labels, see Figure 1.

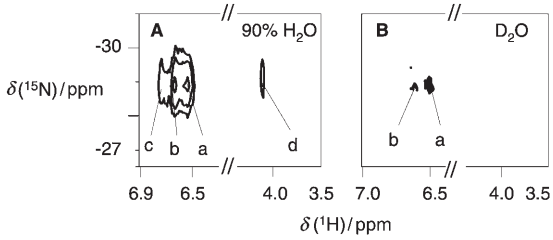

Figure 7. Two-dimensional [^{1}H,^{15}N] HSQC NMR spectra of the 1:1 mixture of duplex **II** and ^{15}N-**2** (0.3 mM, 0.1 M $NaClO_4$ at 283 K, pH 7.0) in (A) 90 % H_2O/10 % D_2O and (B) 100 % D_2O after 5 h of reaction (equilibrium). Assignments: a = en NH(u) of **II**–Ru–G3; b = en NH(u) of **II**–Ru–G6; d = en NH(d) of **II**–Ru–G3 and **II**–Ru–G6; c is not assigned. NH peaks were still detected at ca. 6 ppm for the D_2O solution after 5 h (B), suggesting existence of G-O6···HN-en hydrogen bonding; Ru = [(η^6-biphenyl)Ru(en)]$^{2+}$ (**2**′); for atom labels and structures of **II**–Ru–G3 and **II**–Ru–G6, see Figure 1 and Scheme 1.

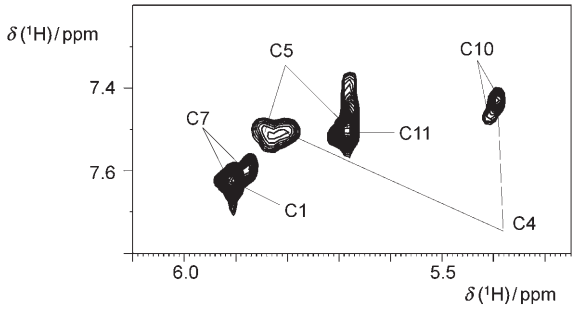

Figure 8. Two-dimensional [^{1}H,^{1}H]-{^{15}N} TOCSY NMR spectrum showing the cytosine H5/H6 cross-peaks for the 1:1 equilibrium mixture of duplex **II** and ^{15}N-**2** (0.3 mM, 0.1 M $NaClO_4$, D_2O, pH 7.0) at 283 K. Note that two sets of resonances are observed for the C4, C5, C7 and C10 residues, suggesting the presence of two monoruthenated products. Assignments are based on the two-dimensional [^{1}H,^{1}H]-{^{15}N} NOESY NMR spectrum (see Figure 9 and Tables 4–6); for DNA sequence, see Scheme 1.

For the second monoruthenated duplex Ru–**II**d a large low-field shift of the H8 resonance was observed for G6 ($\Delta\delta$ = 0.28 ppm), and also for H5 ($\Delta\delta$ = 0.14 ppm) and H1′ ($\Delta\delta$ = 0.38 ppm) resonances of the neighbouring C5 base, but high-field shifts were observed for the H5 ($\Delta\delta$ = −0.08 ppm) and H2″ ($\Delta\delta$ = −0.14 ppm) resonances of C7 in the complementary strand (paired with G6; Table 5). Weak NOE cross-peaks were found between G6-H8 and **2**′-Ho and **2**′-Ho′ protons, between G6-H1′ and **2**′-Ho′, and between C5-H1′ and **2**′-Ho′ protons (Figure 9 and Table 6).

One set of signals was detected from the non-coordinated phenyl ring B of bound fragment [(η^6-biphenyl)Ru(en)]$^{2+}$ (**2**′) in the mixture **II** + **2**, but two sets of signals were observed for the coordinated ring A (Table 6). Compared to unbound **2**, **2**′-Ho′, **2**′-Hp′ and **2**′-Hm′ resonances of ring B were shifted upfield by between 0.48 and 0.63 ppm, the largest shift being for **2**′-Hm′ ($\Delta\delta$ = −0.63 ppm). For ring A, the change in shift of **2**′-Ho resonances was very small. However, **2**′-Hp resonances were shifted upfield by 0.37 (Ru–**II**c) or 0.44 ppm (Ru–**II**d), and the **2**′-Hm resonances shifted downfield by 0.55 (Ru–**II**c) or 0.61 ppm (Ru–**II**d). One set of unshifted signals for **2**′-en CH_2 for both Ru–**II**c and Ru–**II**d was detected. No signals from unreacted ruthenium complex **2** were observed in the equilibrium mixture.

Assignments for ^{1}H NMR peaks of Ru–**II**c and Ru–**II**d in the mixture (**II** + **2**) are shown in Tables 4 and 5, and intermolecular NOE contacts in Figure 9 and Table 6. For Ru–**II**c, a large low-field shift of the G3-H8 resonance was observed ($\Delta\delta$ = 0.40 ppm). The same was also true for H5 ($\Delta\delta$ = 0.39 ppm) and H1′ ($\Delta\delta$ = 0.08 ppm) resonances of the neighbouring C4 base, but high-field shifts were observed for the H1′ resonances of C10 paired with G3 in the complementary strand ($\Delta\delta$ = −0.08 ppm, Table 4). Weak NOE cross-peaks were observed between G3-H8 and the coordinated arene **2**′-Ho and non-coordinated phenyl **2**′-Ho′ protons, between G3-H1′ and **2**′-Ho′, and between C4H1′ and **2**′-Ho′ protons (Figure 9 and Table 6; for atom labelling, see Figure 1).

Table 4. ^{1}H NMR chemical shifts for product Ru–**II**c in the 1:1 equilibrium mixture of duplex **II** and **2** (at 283 K; Ru = [(η^6-biphenyl)Ru(en)]$^{2+}$).

Residue[a]	Proton[b]							
	H8	H6	H5	H1′	H2′	H2″	H3′	H4′
C1		7.66	5.95	5.76	1.93	2.40	4.75	4.09
G2	7.96			5.56	2.77	2.77	5.04	4.34
G3	8.30 (0.40)[c]			6.06	2.69	2.81	n.a.[d]	4.21
C4		7.52 (0.07)	5.81 (0.39)	6.11 (0.08)	2.08	2.40 (−0.09)	4.85	4.22
C5		7.51	5.69	5.62	2.04	2.36	4.90	4.14
G6	8.00			6.22	2.67	2.40	4.75	4.24
C7		7.66	5.95	5.76	1.93	2.40	4.75	4.09
G8	7.96			5.56	2.77	2.77	5.04	4.34
G9	7.90			6.02	2.70	2.77	5.07	4.46
C10		7.49	5.42	5.95 (−0.08)	2.25 (0.15)	2.72 (0.23)	5.05 (0.17)	4.07 (−0.18)
C11		7.54	5.73	5.62	2.04	2.36	4.88	4.14
G12	8.00			6.22	2.67	2.40	4.75	4.24

[a] For DNA sequence, see Scheme 1. [b] For atom labels, see Figure 1. [c] Values in brackets are chemical shift changes from free **II** (see Table S3 in the Supporting Information) of $\geq$0.05 ppm [$\Delta\delta = \delta$(Ru–**II**c)$-\delta$(**II**)]. [d] n.a. = not assigned. **2**′ is bound at N7 of G3.

Table 5. ^{1}H NMR chemical shifts for product Ru–**II**d in the 1:1 equilibrium mixture of duplex **II** and **2** (at 283 K; Ru = [(η^6-biphenyl)Ru(en)]$^{2+}$).

Residue[a]	Proton[b]							
	H8	H6	H5	H1′	H2′	H2″	H3′	H4′
C1		7.66	5.95	5.76	1.93	2.40	4.75	4.09
G2	7.96			5.56	2.77	2.77	5.04	4.34
G3	7.89			6.01	2.70	2.77	5.07	n.a.[c]
C4		7.48	5.51	6.02	2.09	2.48	4.90	4.24
C5		7.52	5.86 (0.14)[d]	6.03 (0.38)	2.27 (0.20)	2.66 (0.27)	4.87	4.24 (0.10)
G6	8.30 (0.28)			6.09 (-0.15)	2.89 (0.19)	2.41	4.84 (0.10)	4.21
C7		7.61 (−0.05)	5.88 (−0.08)	5.74	1.92	2.28 (−0.14)	4.72	4.00 (−0.09)
G8	7.96			5.56	2.77	2.77	5.04	4.34
G9	7.90			6.02	2.70	2.77	5.07	4.46
C10		7.48	5.47	6.02	2.09	2.48	4.90	4.24
C11		7.54	5.73	5.62	2.04	2.36	4.88	4.14
G12	8.00			6.22	2.67	2.40	4.75	4.24

[a] For DNA sequence, see Scheme 1. [b] For atom labels, see Figure 1. [c] n.a. = not assigned. [d] Values in brackets are chemical shift changes from free **II** (see Table S3 in the Supporting Information) of $\geq$0.05 ppm [$\Delta\delta = \delta$(Ru–**II**d)$-\delta$(**II**)]. **2**′ is bound at N7 of G6.

*Diruthenated duplex **II**–Ru$_2$*: Figure S6 in the Supporting Information shows the aromatic and imino proton resonance regions of the ^{1}H NMR spectra of DNA duplex **II** and the diruthenated duplex **II**–Ru$_2$ (Ru = [(η^6-biphenyl)Ru(en)]$^{2+}$ (**2**′)). This diruthenated duplex was obtained by annealing the monoruthenated single-strand **I** collected by HPLC (**I**–Ru–G3; Scheme 1 and Figure 2). The broadening and intensity decrease of the imino proton resonances was notable.

The two-dimensional [^{1}H,^{15}N] HSQC NMR spectrum of **II**–Ru$_2$ at 283 K in 90% H$_2$O/10% D$_2$O (Figure 10) gave rise to two cross-peaks at δ = 6.62/−27.17 ppm, assignable to en-NHu, and δ = 4.20/−27.17 ppm, assignable to en-NHd resonance of **2**′ (Table S2 in the Supporting Information). After lyophilisation and re-dissolution of this sample in D$_2$O, no NH peaks were detected.

Figure 11 shows the two-dimensional [^{1}H,^{1}H] TOCSY NMR spectrum in the cytosine H5/H6 cross-peak region for **II**–Ru$_2$ (1.1 mM, 0.1 M NaClO$_4$) in D$_2$O at 283 K. Two sets of resonances were observed for the C1, C4, C7 and C10 residues, suggesting the presence of a diruthenated product as well as a very small amount of duplex **II**. The sugar ring H1′ (6.4–5.4 ppm) to H2′ and H2″ (3.0–1.7 ppm) TOCSY connectivities of duplex **II** and **II**–Ru$_2$ are shown in Figure 12. The H1′/H2″ cross-peaks for C4 and C10 residues in **II**–Ru$_2$ were shifted compared with free duplex **II** to give new broad peaks, but H1′/H2″ cross-peaks for G3 and G9 residues in **II**–Ru$_2$ were too broad to assign. Decreased intensities of the H1′/H2′ and H1′/H2″ cross-peaks were found for C5, C11, G2 and G8 residues, but not for C1, C7, G6 and G12 residues.

Assignments for ^{1}H NMR cross-peaks of diruthenated duplex **II**–Ru$_2$ are shown in Table 7, and NOE contacts are listed in Table 8. Large low-field shifts of the G3-H8 and G9-H8 resonances were observed ($\Delta\delta$ = 0.43 and 0.36 ppm, respectively), as was also the case for the H5 resonances of the neighbouring residues C4 ($\Delta\delta$ = 0.68 ppm) and C10 ($\Delta\delta$ = 0.68 ppm). The largest changes in H1′ chemical shifts occurred for the C4 and C10 residues (both $\Delta\delta$ = −0.19 ppm). Weak cross-peaks were found between G3-H2″, G3-H2′, G9-H2″, G9-H2′ and **2**′-Ho arene protons, between G3-H2″, G3-H1′, G9-H2″, G9-H1′, C4-H1′, C10-H1′ and **2**′-Ho′ protons, and between C4-H1′, C10-H1′ and **2**′-Hp′ protons (Figure 13 and Table 8).

Two sets of signals were observed for the coordinated phenyl ring A, but only one set of signals for the non-coordinated phenyl ring B for the two bound fragments **2**′ in **II**–Ru$_2$ (Table 8). Relative to unbound **2** (in aqua species H$_2$O-**2**), the **2**′-Ho′, **2**′-Hp′ and **2**′-Hm′ resonances of ring B were shifted upfield by 0.41 to 0.52 ppm, and the largest shift was for **2**′-Hm′ ($\Delta\delta$ = 0.52 ppm). For ring A, little change occur-

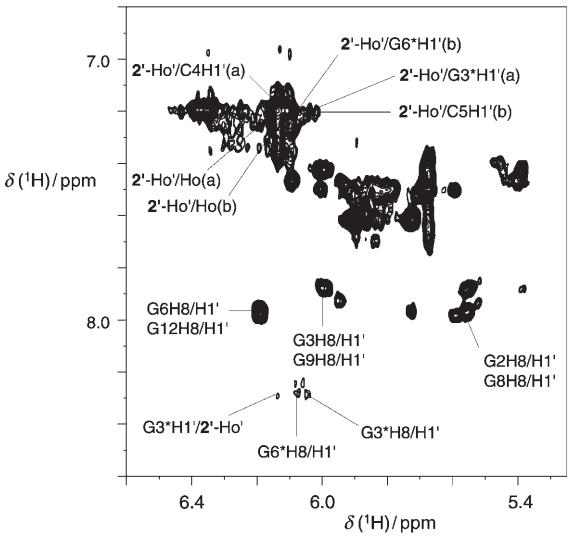

Figure 9. Part of the two-dimensional [^{1}H,^{1}H]-{^{15}N} NOESY NMR spectrum of the 1:1 equilibrium mixture of duplex **II** and ^{15}N-**2** (0.3 mM, 0.1 M $NaClO_4$, 283 K, pH 7.0, mixing time 400 ms) in D_2O. The interresidue $[(\eta^6\text{-biphenyl})Ru(en)]^{2+}$–**II** cross-peaks observed for the monoruthenated product **II**–Ru–G3 are: G3*H8/**2**′-Ho′(a), G3*H1′/**2**′-Ho′(a) and **2**′-Ho′/C4H1′(a); and for **II**–Ru–G6 are: G6*H8/**2**′-Ho′(b), G6*H1′/**2**′-Ho′(b) and **2**′-Ho′/C5H1′(b). Cross-peaks observed within the ruthenated guanine residues G3* or G6*, and within the bound ruthenium complex **2**′ are also indicated. Labels: **2**′ = $[(\eta^6\text{-biphenyl})Ru(en)]^{2+}$; ruthenated guanines are marked with asterisks; for NMR chemical shifts, see Tables 4–6, and atom labels, see Figure 1.

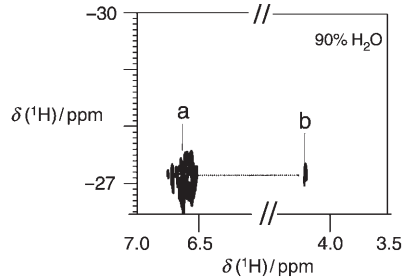

Figure 10. Two-dimensional [^{1}H,^{15}N] HSQC NMR spectrum of the diruthenated duplex **II**–Ru_2–G3G9 (1.1 mM, 0.1 M $NaClO_4$) in D_2O at 283 K; Ru = $[(\eta^6\text{-biphenyl})Ru(^{15}N\text{-en})]^{2+}$ (^{15}N-**2**′). Assignments: a = en NH(u) resonances of **II**–Ru_2–G3G9; b = en NH(d) resonances of **II**–Ru_2–G3G9. No NH peaks were detected for D_2O solutions. It is notable that in a similar duplex monoruthenated with $[(\eta^6\text{-}p\text{-cymene})Ru(en)]^{2+}$ (**1**′), the NH peaks are still detectable in the D_2O solution (Figure 4). This suggests that the G-O6···HN-en hydrogen bonds in **II**–Ru_2–G3G9 are weakened due to intercalation of the biphenyl ligand. For the monoruthenated **II** (**II**–Ru–G3 and **II**–Ru–G6), the en NH(u) resonances are also detectable in D_2O (Figure 7), though they are weakened compared with those in 90% H_2O. It is possible that double ruthenation mediates hydrogen bonding further, see discussion section. For atom labels and structure of **II**–Ru_2–G3G9, see Figure 1 and Scheme 1.

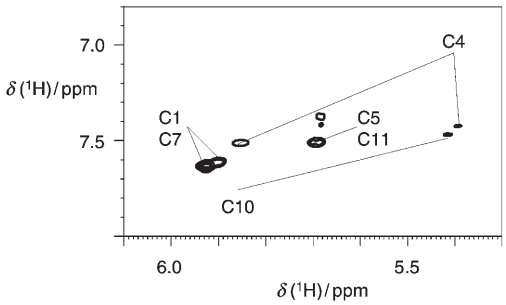

Figure 11. Two-dimensional [^{1}H,^{1}H]-{^{15}N} TOCSY NMR spectrum in the cytosine H5/H6 cross-peak region for the diruthenated duplex **II**–Ru_2–G3G9 (1.1 mM, 0.1 M $NaClO_4$) in D_2O at 283 K; Ru = $[(\eta^6\text{-biphenyl})Ru(en)]^{2+}$ (**2**′). Note that two sets of resonances are observed for the C1, C4, C7 and C10 residues suggesting the presence of a diruthenated product as well as a small amount of unreacted duplex **II**. Assignments are based on the two-dimensional [^{1}H,^{1}H]-{^{15}N} NOESY NMR spectrum (see Figure 13 and Tables 7 and 8); for DNA sequence, see Scheme 1.

red for the **2**′-Ho resonance. However, the resonances of **2**′-Hp were shifted upfield by 0.35 (for **2**′ bound to G3) or 0.28 ppm (for **2**′ bound to G9), and those of **2**′-Hm downfield by 0.49 (for **2**′ bound to G3) or 0.59 ppm (for **2**′ bound to G9). One set of unshifted signals for en CH_2 of **2**′ was detected.

Reaction of single strand I with complex 1 or 2: The reaction mixtures of ss-DNA **I** with ^{15}N-**1** (1:6) or ^{15}N-**2** (1:4) in 90% H_2O/10% D_2O at 283 K were also studied by one- and two-dimensional NMR spectroscopy. Spectra for the reaction mixture of **I**+**1** are shown in Figure S7 in the Supporting Information and assignments are given in Tables S2, S5 and S6 in the Supporting Information. The two-dimensional [^{1}H,^{15}N] HSQC NMR spectrum (data not shown) of the mixture contained three species: the chloro complex **1**, aqua complex H_2O-**1** and triruthenated single strand adduct **I**–Ru_3 (Ru = $[(\eta^6\text{-}p\text{-cymene})Ru(en)]^{2+}$ (**1**′))

Table 6. ^{1}H NMR chemical shifts for $[(\eta^6\text{-biphenyl})Ru(en)Cl][PF_6]$ (**2**) and bound fragment $[(\eta^6\text{-biphenyl})Ru(en)]^{2+}$ (**2**′), and intermolecular NOEs in the 1:1 equilibrium mixture of duplex **II** and **2** (at 283 K).

Proton[a]		Ru–**II**c			Ru–**II**d		
	2	**2**′	Δδ[b]	NOEs (**II**-**2**′)[c]	**2**′	Δδ[b]	NOEs (**II**-**2**′)[c]
en-CH_2	2.36 2.45	2.47			2.47		
en-NHd	4.14	n.a.[d]			n.a.[d]		
Ho	6.20	6.15	−0.05	G3*H8(w)[e]	6.12	−0.08	G6*H8 (w)
Hp	6.10	5.73	-0.37		5.66	−0.44	
Hm	5.93	6.48	0.55		6.54	0.61	
Ho′	7.81	7.21	−0.60	G3*H8(w) G3*H1′(w) C4H1′(w)	7.21	−0.60	G6*H8 (w) G6*H1′ (w) C5H1′ (w)
Hp′	7.61	7.13	−0.48		7.13	−0.48	
Hm′	7.61	6.98	−0.63		6.98	−0.63	
en-NHu	6.19	6.61	0.42		6.55	0.36	

[a] For atom labels and DNA sequence, see Figure 1 and Scheme 1. [b] $\Delta\delta = \delta(\mathbf{2}') - \delta(\mathbf{2})$ (≥ 0.05 ppm). [c] **2**′ is bound at G3N7 or G6N7, and the ruthenated guanines are marked with asterisks. [d] n.a. = not assigned. [e] s = strong, m = medium, w = weak.

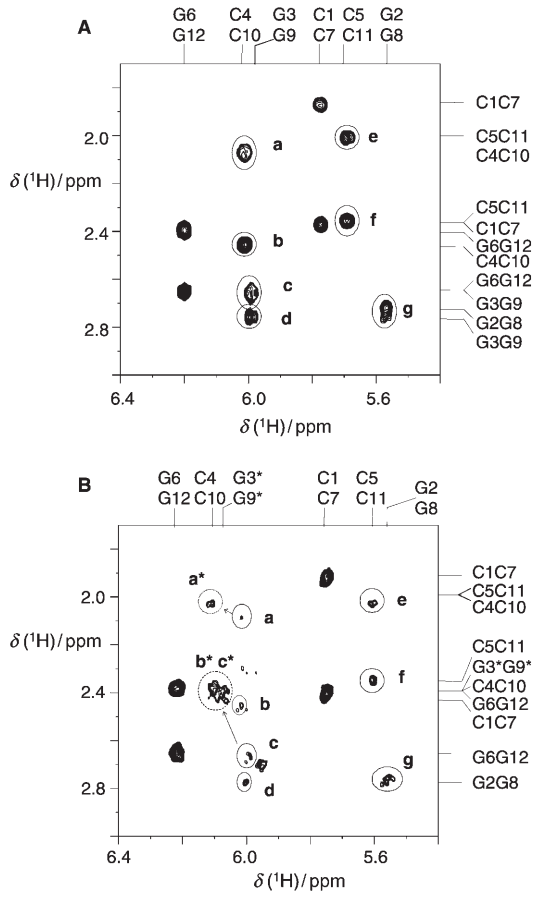

Figure 12. Two-dimensional [^{1}H,^{1}H]-{^{15}N} TOCSY NMR spectra of A) duplex **II** and B) the diruthenated duplex **II**–Ru_2–G3G9 (1.1 mM, 0.1 M $NaClO_4$ in D_2O, at 283 K and pH 7.0, mixing time 80 ms), showing the sugar ring H1′ (6.4–5.4 ppm) to H2′ and H2″ (3.0–1.7 ppm) connectivities; Ru = [(η^6-biphenyl)Ru(en)]$^{2+}$ (**2′**). The circles indicate C-H1′/H2′ and C-H1′/H2″ or G-H1′/H2′ and G-H1′/H2″ cross-peaks: a, C4/C10-H1′/H2′; b, C4/C10-H1′/H2″; c, G3/G9-H1′/H2′; d, G3/G9-H1′/H2″; e, C5/C11-H1′/H2′; f, C5/C11-H1′/H2″; g, G2/G8-H1′/H2′ and G2/G8-H1′/H2″. Note the downfield shift of cross-peaks a, b and c to give a*, b* and c*, respectively and decrease in intensity of cross-peaks e, f and g after ruthenation of G3*N*7 and G9*N*7. For DNA sequence, see Scheme 1.

(Table S2 in the Supporting Information). In the one-dimensional spectra of **I** in the presence of six molar equivalents of **1** (Figure S7 in the Supporting Information), the binding of [(η^6-*p*-cymene)Ru(en)]$^{2+}$ was indicated by the large low-field shift of all the guanine H8 resonances (0.51–0.66 ppm) and the cytosine H6 and H5 resonances (0.12–0.60 ppm) (Table S5 in the Supporting Information). Compared to free **1**, **1**′-CH_3b, **1**′-CH and **1**′-CH_3a ^{1}H resonances were shifted to high field (by 0.14–0.31 ppm), and **1**′-Ha/Ha′ proton resonances were shifted to low field (by 0.06 ppm); the **1**′-en CH_2 proton resonances were unshifted. The largest shift was for **1**′-CH (Table S6 in the Supporting Information).

The ^{1}H NMR spectra for the reaction mixture of **I**+**2** are shown in Figure S8 in the Supporting Information and assignments are shown in Tables S2, S7 and S8 in the Supporting Information. The two-dimensional [^{1}H,^{15}N] HSQC NMR spectrum (data not shown) of the mixture showed the presence of three species: **2**, H_2O-**2** and triruthenated single strand adduct **I**–Ru_3 (Ru = [(η^6-biphenyl)Ru(en)]$^{2+}$ (**2′**)) (Table S2 in the Supporting Information). The binding of [(η^6-biphenyl)Ru(en)]$^{2+}$ is indicated by the large low-field shift of all the G-H8 resonances (0.49–0.61 ppm) and the C-H6 and C-H5 resonances (0.12–0.47 ppm) (Table S7 in the Supporting Information). There was only one set of signals from the non-coordinated phenyl ring B of the bound fragment **2′**, and there were three sets of signals from the ring A. Relative to free **2**, **2′**-Ho′, **2′**-Hp′ and **2′**-Hm′ resonances of non-coordinated ring B were shifted to high field (0.34–0.41 ppm), the largest shift was for **2′**-Ho′; but for ring A, **2′**-Hp was shifted to high field (0.29 ppm), and the **2′**-Ho (0.07–0.18 ppm), and **2′**-Hm (0.48–0.55 ppm) resonances to low field.

Discussion

Reverse-phase HPLC together with ESI-MS allowed separation and identification of mono-, di- and triruthenated DNA hexamers formed during reactions of the single-strand d(CGGCCG) or duplex $d(CGGCCG)_2$ with Ru^{II}–arene anticancer complexes [(η^6-arene)Ru(en)Cl]$^+$ (arene = *p*-cymene (**1**) or biphenyl (**2**)).[1,16] Even isomeric ruthenated DNA adducts were readily separated by HPLC. Since the ruthenating fragment [(η^6-arene)Ru(en)]$^+$ is relatively hydrophobic, the greater the extent of ruthenation of the DNA, the longer was the retention time, which also depended on the position of the ruthenation in the sequence.

Adducts of duplex **II** eluted as single strands from the reverse-phase HPLC column (Figure 2d). This has often been observed for reactions of duplex DNA with platinum anticancer complexes.[17] For example, 3′-G and 5′-G platinated single-strand monoadducts and the GG-chelate adducts have been separated on a C18 reverse-phase column from the 1:1 reaction mixture of the duplex $d(TTGGCCAA)_2$ with *cis*-[$Pt(NH_3)_2(H_2O)_2$]$^{2+}$ and [$Pt(NH_3)_3(H_2O)$]$^{2+}$. [Pt(dien)Cl]$^+$ adducts of 10- and 12-mer duplexes have been separated by anion exchange chromatography.[12] The increase in hydrophobicity, together with partial charge neutralisation of the ruthenated DNA probably accounts for the observed precipitation of triruthenated single-strand adducts at concentrations higher than 0.20 mM, and when more than one molar equivalent of **1** or **2** was added to duplex **II** (0.2 mM). Three monoruthenated products were detected for reactions of single strand **I** with **1** or **2** at a Ru/**I** mol ratio of 0.5:1, but only two monoruthenated products for reactions of duplex **II** with **1** or **2** at a Ru/**II** mol ratio of 1:1, indicating that the ruthenation of duplex **II** is base- *and* sequence-selective.

The pattern of ruthenation of single strand DNA **I** by **1** and **2** was similar (Figure 2a–c). However, the biphenyl complex **2** is much more reactive towards the duplex **II** than is the *p*-cymene complex **1**, as has been observed previously with calf thymus DNA.[5]

Table 7. ^{1}H NMR chemical shifts for the nucleotides in diruthenated duplex **II**–Ru_2 (at 283 K; Ru = [(η^6-biphenyl)Ru(en)]$^{2+}$).

Residue[a]	Proton[b]							
	H8	H6	H5	H1′	H2′	H2″	H3′	H4′
C1		7.62	5.92	5.74	1.92	2.40	4.71	4.07
G2	7.98			5.56	2.77	2.77	5.00	4.33
G3	8.33			6.07	2.38	2.67	n.a.[d]	4.18
	(0.43)[c]				(−0.32)	(−0.12)		(−0.32)
C4		7.48	6.10	5.84	2.03	2.39	4.82	4.19
			(0.68)	(−0.19)	(−0.07)	(−0.10)	(−0.06)	(−0.06)
C5		7.53	5.69	5.60	2.03	2.39	4.82	4.11
G6	7.99			6.21	2.66	2.39	4.70	4.21
C7		7.62	5.92	5.74	1.92	2.40	4.71	4.07
G8	7.98			5.56	2.77	2.77	5.00	4.33
G9	8.26			6.04	2.38	2.67	n.a.	4.16
	(0.36)				(−0.32)	(−0.12)		(−0.34)
C10		7.48	6.10	5.84	2.03	2.39	4.82	4.19
			(0.68)	(−0.19)	(−0.07)	(−0.10)	(−0.06)	(−0.06)
C11		7.53	5.69	5.60	2.03	2.39	4.82	4.11
G12	7.99			6.21	2.66	2.39	4.70	4.21

[a] For DNA sequence, see Scheme 1. [b] For atom labels, see Figure 1. [c] Values in brackets are chemical shift changes from free **II** (see Table S3 in the Supporting Information) of ≥0.05 ppm [$\Delta\delta = \delta$(**II**–Ru_2) - δ(**II**)]. [d] n.a. = not assigned. **2′** is bound at N7 of G3 and G9.

Table 8. ^{1}H NMR chemical shifts for [(η^6-biphenyl)Ru(en)(H_2O)]$^{2+}$ (H_2O-**2**) and G3 or G9 bound fragment [(η^6-biphenyl)Ru(en)]$^{2+}$ (**2′**-G3 or **2′**-G9), and NOEs between arene and DNA protons in the diruthenated duplex **II**–Ru_2 (at 283 K, Ru = [(η^6-biphenyl)Ru(en)]$^{2+}$)

Proton[a]	H_2O-**2**	**2′**-G3/**2′**-G9	$\Delta\delta$[b] G3/G9	NOEs (**II**-**2′**)[c]
en-CH_2	2.44	2.46		
en-NHd	4.02	n.a.[c]		
Ho	6.14	6.17/6.17		G3*H2′ (w)[d]/G9*H2′ (w)
				G3*H2″ (w)/G9*H2″ (w)
Hp	5.97	5.62/5.69	−0.35/−0.28	
Hm	5.88	6.37/6.47	0.49/0.59	
Ho′	7.77	7.27/7.27	−0.50/−0.50	G3*H1′ (w)/G9*H1′ (w)
				C4H1′ (w)/C10H1′ (w)
				G3* H2″ (w)/G9*H2″
Hp′	7.57	7.16/7.16	−0.41/−0.41	C4H1′ (w)/C10H1′ (w)
				C4H2′ (w)/C10H2′ (w)
				C4H2″ (w)/C10 H2″ (w)
Hm′	7.57	7.05/7.05	−0.52/−0.52	
en-NHu	6.04	6.50/6.50	−0.46/−0.46	

[a] For atom labels and DNA sequence, see Figure 1 and Scheme 1. [b] $\Delta\delta = \delta$(**2′**)−δ(H_2O-**2**) (≥0.05 ppm). [c] n.a. = not assigned. [d] s = strong, m = medium, w = weak. [e] **2′** is bound at G3N7 and G9N7 and the ruthenated guanines are marked with asterisks.

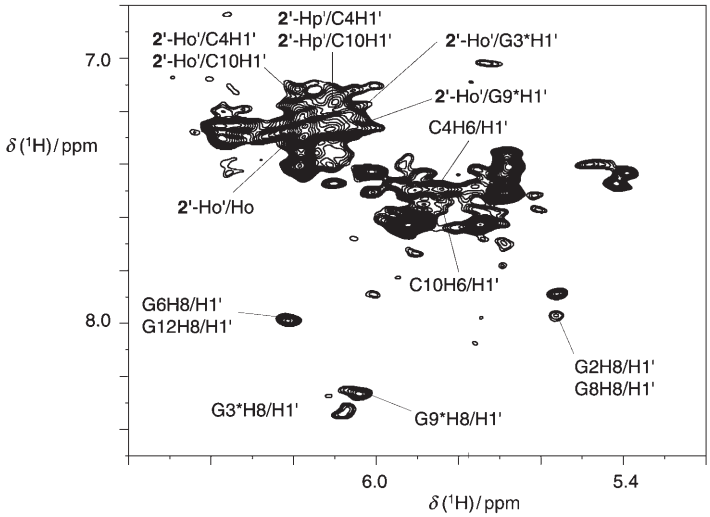

Figure 13. Part of the two-dimensional [^{1}H,^{1}H]-{^{15}N} NOESY NMR spectrum of the diruthenated duplex **II**–Ru_2–G3G9 (1.1 mM, 0.1 M $NaClO_4$ in D_2O, at 283 K and pH 7.0, mixing time 400 ms); Ru = [(η^6-biphenyl)Ru(en)]$^{2+}$ (**2′**). Intra-residue and [(η^6-biphenyl)Ru(en)]$^{2+}$–**II** cross-peaks arising from NOEs between ruthenated guanine residues G3* or G9* and the bound ruthenium complex **2′** are indicated. Labels; resonances for ruthenated guanine are marked with asterisks; for NMR chemical shifts, see Table 7 and Table 8, and for atom labels, see Figure 1.

Determination of the binding sites by NMR spectroscopy: Previous studies of reactions of [(η^6-arene)Ru(en)Cl]$^+$ complexes with nucleobases[6] have shown that the reactivity decreases in the order G(N7) > T(N3) > C(N3) > A(N7), A(N1), and in competitive reactions of nucleotides binding only to G is observed. For the single-strand 14-mer d(ATACATGGTACATA), complex **1** binds strongly and selectively to the central G bases forming monofunctional adducts.[1]

Selective binding to N7 of the G residues of the 6-mer DNA used here was evident from the ^{1}H NMR chemical shift changes. Binding of Ru–arene complexes **1** or **2** to 5′-GMP[1,6] through N7 caused a low-field shift of the H8 ^{1}H NMR resonance by up to 0.7 ppm. Similar shifts were observed for the H8 resonances of G bases in the hexamer, duplex **II**–Ru_2 (Ru = [(η^6-biphenyl)Ru(en)]$_2$ (**2′**), Table 7), indicate that the binding sites for **2′** in the duplex are G3N7 and G9N7, and thus the duplex **II**–Ru_2 is assigned as **II**–Ru_2–G3G9(**2′**).

The low-field shifts of all G-H8 resonances (by up to 0.66 ppm) in the 1:6 mixture of **I**+**1** and in 1:4 mixture of **I**+**2** (Tables S5 and S7 in the Supporting Information), indicate that under these conditions all G N7s are ruthenated by **1′** or **2′** to form triruthenated single strand DNA adducts **I**–Ru_3–G2G3G6(**1′**) and **I**–Ru_3–G2G3G6(**2′**).

and allow assignment of the binding sites as G3 in Ru–**II**a and G6 in Ru–**II**b formed from the reaction of **II**+**1**, G3 in Ru–**II**c and G6 in Ru–**II**d formed from the reaction of **II**+**2** (Tables 1, 2, 4 and 5). If the binding fragment [(η^6-*p*-cymeme)Ru(en)]$^{2+}$ is labelled as **1′** and [(η^6-biphenyl)-Ru(en)]$^{2+}$ as **2′**, then the monoruthenated duplex Ru–**II**a is assigned as **II**–Ru–G3(**1′**), Ru–**II**b as **II**–Ru–G6(**1′**), Ru–**II**c as **II**–Ru–G3(**2′**), and Ru–**II**d as **II**–Ru–G6(**2′**) (for DNA sequence, see Scheme 1).

The low-field shifts of the H8 resonances of G3 and G9 by up to 0.40 ppm in the diruthenated

Duplex ruthenation was also accompanied by selective changes in imino proton resonances: those of G3 in **II**–Ru–G3(**1′**), and G6 in **II**–Ru–G6(**1′**) shifted to high field by 0.19 and 0.11 ppm, respectively. Platination of the 14-mer duplex d(TATGTACCATGTAT)/d(ATACATGGTACATA) also causes high field shifts of G imino proton resonances.[14] As with platination,[14] ruthenation also affects the resonances of neighbouring bases: large low-field shifts of the H5 and H6 resonances are observed for C4 in **II**–Ru–G3(**1′**) and C5 in **II**–Ru–G6(**1′**), of H5 for C4 in **II**–Ru–G3(**2′**) and C5 in **II**–Ru–G6(**2′**), and also for the C4 and C10 bases in **II**–Ru_2–G3G9(**2′**) (Tables 1, 2, 4, 5 and 7).

Intercalation: We sought to determine whether the biphenyl ligand in **2** could intercalate into the hexamer duplex in contrast to the *p*-cymene ligand in **1**, which cannot intercalate. Literature reports show that intercalation into DNA base-pairs often results in upfield ^{1}H NMR shifts of resonances of the intercalator,[18–23] and the interruption or weakening of NOE connectivities between sequential DNA nucleotides.[18,19,21] NOE cross-peaks between protons of the intercalator and those of DNA have been observed at sites of intercalation,[21,22] and peaks for H1′ and H2′/H2″ sugar protons at the intercalated base steps are shifted upfield.[18,19,23] The DNA melting temperature (T_m) usually increases after intercalation.[18–23]

For the *p*-cymene complex, the CH_3a, CH_3b and CH ^{1}H NMR resonances of bound **1′** in both **II**–Ru–G3(**1′**) or **II**–Ru–G6(**1′**) were shifted to high field by −0.16 to −0.32 ppm. However, the en-CH_2 ^{1}H resonances were shifted to low field and the arene ring Ha/Ha′ and Hb/Hb′ proton resonances changed little (Table 3). Interruptions of the sequential NOE connectivities between the G3 and C4 in **II**–Ru–G3(**1′**), and between the C5 and G6 in **II**–Ru–G6(**1′**) were observed. Interresidue NOE cross-peaks were observed only between protons of bound fragment **1′** and residues G3 or G6. Also the H1′ and H2′/H2″ sugar protons of G3 and G6 were shifted to low field (Tables 1 and 2). These data are consistent with the lack of intercalation of *p*-cymene, which has bulky methyl and isopropyl substituents, in adducts **II**–Ru–G3(**1′**) and **II**–Ru–G6(**1′**), as expected.[5]

Experiments carried out in D_2O revealed the retention of en-N*H* for a monitored period of 72 h, slow NH/ND exchange being attributable to the presence of hydrogen bonding between G3O6 and en-NH. This can occur only if the en ligand is oriented such that en-NH comes into close contact with G3-O6.

Large upfield shifts of 0.41–0.63 ppm for all proton resonances of the non-coordinated phenyl ring B of **2′** were found for monoruthenated duplexes **II**–Ru–G3(**2′**) and **II**–Ru–G6(**2′**) (Table 6), and also for diruthenated **II**–Ru_2–G3G9(**2′**) (Table 8). These shifts are attributable to shielding effects from the ring currents of nucleobases that form a sandwich with the intercalated phenyl ring B of bound **2′**. Such shielding is commonly considered as evidence for an intercalative binding mode.[18–27] For example, upfield shifts of a similar magnitude (0.4–1.0 ppm) have been reported for intercalated acridine.[18,19] NOE cross-peaks were found not only between ring B of bound **2′** and H1′ and H8 protons of G3 in **II**–Ru–G3(**2′**), but also between ring B and H1′ of C4 (Table 6). This can occur only if the intercalation occurs at the G3pC4 base step. Analogous NOE cross-peaks between ring B of bound **2′** and H1′ and H8 of G6 and H1′ of C5 were found for **II**–Ru–G6(**2′**), indicating that intercalation occurs between G6 and C5 (Table 6). For the diruthenated duplex **II**–Ru_2–G3G9(**2′**), NOE cross-peaks were detected not only between ring B of bound **2′** and H1′ and H2′/H2″ of G3 and H1′ of C4, but also between ring B and H1′ of C10 and H1′ and H2′/H2″ of G9, indicating the presence of intercalation sites between G3 and C4, and between C10 and G9 (Table 8). The interruption of NOE connectivities between the corresponding base-pairs is consistent with these intercalation sites. Intercalation of acridin-9-ylthiourea into $d(GGACGTCC)_2$ or $d(GGAGCTCC)_2$ gives rise to upfield shifts of some of the H1′ and H2′/H2″ sugar protons at the intercalation base steps.[18] Such upfield shifts (up to $\Delta\delta = -0.32$ ppm) are also observed for the H1′ and H2′/H2″ protons of G3/C4 and G9/C10 at the proposed intercalation sites of the diruthenated duplex **II**–Ru_2–G3G9 (Table 7) caused by ring current effects of the intercalated phenyl ring.

In **II**–Ru–G3(**2′**), **2′** is eventually oriented in such a way that a G3-O6 to en-NH hydrogen bond is less likely to form compared with **II**–Ru–G3(**1′**), consistent with the weak en-NH resonances observed for **II**–Ru–G3(**2′**) in D_2O (Figure 7). Resonances for Ho′, Hp′ and Hm′ of **2′** are consistently shielded relative to free **2**, consistent with the base stacking of the non-coordinated phenyl ring. The data implicate biphenyl as an aggressive ligand, the non-coordinated ring B pushing through the major groove deep enough to give rise to NOE contacts between protons of ring B and H1′ and H2′/H2″ protons of G3 and in particular between Hp′ of **2′** and the H1′ proton of residue C4, together with changes in the H4′ proton chemical shifts at the intercalation sites (see Table 5). The driving force for the intercalation is likely to arise from the hydrophobic nature of the non-coordinated phenyl ring, which would tend to bury itself within the DNA base stack rather than be exposed to solvent in the major groove. This tendency is then likely to be stabilised by π–π interactions within the G3–phenyl ring–C4 or the G9–phenyl ring–C10 "sandwich". This intercalation distorts the DNA and reduces the strength of hydrogen bonding between en-NH and G3-O6. It was reported[9,18–27] that the GpC site is the preferred intercalation binding site for actinomycin D (ActD) ligands and, moreover, the flanking sequences at the GpC binding site play an important role in the binding affinity of this intercalator. It is interesting in the present work that all of the intercalation occurs between GpC base steps, and there is no evidence for intercalation at the GpG base steps. This may be due to the lessening of steric crowding at the GpC step relative to the GpG step, thereby allowing accommodation of the arene ring. A further driving force for GpC rather than GpG intercalation is the weaker purine–pyrimidine π–π stacking inter-

action for GpC compared to purine-purine GpG steps.[28] It is therefore likely that intercalation at GpC by **2′** has a lower energy penalty when compared with intercalation at GpG base steps.

In the diruthenated duplex **II**–Ru_2–G3G9(**2′**), intercalation is likely between G3/C4 when the biphenyl complex is bound at G3, but this may preclude intercalation at G9/C10 for the Ru biphenyl bound at G9. This would make the duplex unsymmetrical and account for the observation of two sets of NMR peaks, one for each strand.

Dynamics: The intensities of the imino proton resonances for the terminal base-pairs G6·C7 and G12·C1 of the duplex increased after ruthenation at G3 or G6 by the *p*-cymene complex **1′**, whilst those for the inner base-pairs G2·C11, G3·C10, G8·C5 and G9·C4 remained unchanged. This suggests that ruthenation results in a decrease in the opening rate of these base-pairs. In contrast the imino proton resonances of the duplexes **II**–Ru–G3(**2′**) or **II**–Ru–G6(**2′**) and duplex **II**–Ru_2–G3G9(**2′**) became broad and weak, implying that the base-pairs are disrupted in the duplex with an increase in dynamic mobility of the bases. Such perturbations of the structure of the DNA duplex may have implications for protein binding and contribute to mechanism of action of these anticancer complexes.

The effect of intercalation is often to increase the melting temperature (T_m) of DNA duplexes by ≥ 20 K.[18–26] In the current case the melting temperature of the double-intercalated duplex **II**–Ru_2–G3G9(**2′**) ($T_m = 302.3 \pm 0.9$ K, 100 mM $NaClO_4$) is 14 K lower than that of the free duplex **II** ($T_m = 316.8 \pm 0.1$ K), clearly indicative of destablisation of the double helix. Experimentally this would lead to lower intensity imino and amino proton resonances, due to the weakening of interstrand hydrogen bonds, resulting in a duplex that is largely destabilised in the vicinity of the ligand binding site. Isothermal calorimetric studies[29] of monofunctional (G) adducts of the potential intercalating complex $[(\eta^6\text{-tetrahydroanthracene})Ru(en)]^{2+}$ and of the *p*-cymene complex **1** with the 15-mer duplex d(CTCTCTTGTCTTCTC)·d(GAGAAGACAAGAGAG) have shown that the duplex is destabilised enthalpically by 4.4 and 7.4 kcal mol^{-1}, respectively.

Ru–enNH···GO6 hydrogen bonding: Strong stereospecific intramolecular hydrogen bonding between an en NH proton oriented away from the arene (en NHd) and the C6 carbonyl of G is observed in the solid state and implied from NMR data of solutions of $[(arene)Ru(en)]^{2+}$ adducts of model guanine complexes.[6] Such hydrogen bonding partly accounts for the high preference for binding to G versus A (adenine) which lacks a hydrogen-bond acceptor at the 6-position of the purine residue.

For model G adducts with **2**, such as guanosine 5′-monophosphate, Ru-enNH···GO6 hydrogen bonding greatly inhibits NH/ND exchange in D_2O; the hydrogen-bonded NH proton is NH(d). However, this resonance appears close to the water peak and is detectable only over the pH range $6 < pH < 8$, disappearing at pH values < 6 and > 8.[6] For the adducts of complex **1** with duplex **II** studied here (**II**–Ru–G3(**1′**) and **II**–Ru–G6(**1′**), Figure 4), the resonance for NH(d) was too broad to observe even at 283 K. Surprisingly, the exchange of the en-NHu protons was very slow and was reasonably slow for the monointercalated biphenyl duplexes **II**–Ru–G3(**2′**) or **II**–Ru–G6(**2′**) (Figure 7). However, NH exchange was rapid for the en-NH(u) protons in the double-intercalated duplex **II**–Ru_2–G3G9(**2′**) (no $^1H/^{15}N$ cross-peaks being detected for a D_2O solution of **II**–Ru_2–G3G9(**2′**), Figure 10). The slow exchange of NH(u) protons could primarily be rationalised by additional hydrogen-bonding interactions. In all cases the most likely rationale is for hydrogen bonding to occur between en-NH(u) and either nearby phosphodiester backbone residues or hydrogen-bonding acceptors on the complementary DNA strand. For instance hydrogen bonding between en-NH(u) and O2P at the C^1pG^2 step of **II**–Ru–G3(**1′**) could occur through motion of the phosphodiester backbone. For **II**–Ru–G3(**2′**) the arene intercalation forces the en-NH(u) protons into geometrical positions that are much less favourable for hydrogen bonding with either the phosphodiester backbone or with components of the complementary strand.

It is clear that exchange of NH(u) with solvent D is slow on the NMR timescales in specific instances (Figures 3 and 6). Exchange of en-NH_2 protons could occur either by Ru–N bond cleavage or through proton dissociation. It appears therefore that NH(u) hydrogen bonding decreases the lability of NH protons and/or strengthens the Ru–N bond.

Sequence specificity of G metallation: Reactions of complexes **1** and **2** with the duplex **II** $d(CGGCCG)_2$ give rise to little ruthenation of G2. Many studies have been carried out on the specificity of platination of G residues in GG sequences, since attack on GG by cisplatin with subsequent formation of 1,2-intrastrand cross-links leads to DNA bending and HMG protein recognition.[30,31] Exclusive attack on the 3′-G (G3), as seen for these organometallic Ru–arene complexes, is uncommon for platination. For example, only 5′-G platination is found when the monofunctional complex $[Pt(dien)Cl]^+$ (dien = diethylenetriamine) reacts with DNA duplex $d(TATGGCCATA)_2$.[12] The rates of binding of monofunctional *cis*-$[PtCl(H_2O)(NH_3)_2]^+$ or bifunctional *cis*-$[Pt(H_2O)_2(NH_3)_2]^{2+}$ to the 5′-G of the double-strand oligonucleotides are much greater than those for the 3′-G.[32] The pseudo-octahedral coordination site on an [(arene)-(Ru^{II})(en)] complex is more sterically demanding than that of a square-planar site on Pt^{II}, and this may contribute to the difference in sequence specificities. For DNA bases in proximity to the phosphodiester backbone, C (six-membered ring attached through glycosidic bond with H5/H6 exposed in the major groove) is expected to be more sterically demanding than G (five-membered ring attached at the glycosidic bond). The combined steric demands of C plus the Ru^{II} complex are likely to account for a preference in binding to G3-N7 compared to G2-N7. Although both of G2 and G6 follow a cytosine, G2 is also adjacent to a guanine, whereas

G6 is terminal, which implies that there is less steric hindrance around G6 than G2. Therefore G6 is apparently ruthenated while G2 is not.

Conclusion

We have studied the binding of two Ru^{II}–arene complexes to single- and double-stranded DNA. The *p*-cymene complex **1** (IC_{50} 10 μM) is less cytotoxic to A2780 ovarian cancer cells than the biphenyl complex **2** (IC_{50} 5 μM).[2] We have previously shown that the arene can exert a significant effect on the chemical reactivity of these Ru^{II} complexes and on distortions induced in DNA.[5,29,33] For example the rate of reaction of **1** with cGMP is approximately three times slower than that of **2**,[7] and the biphenyl complex **2** induces an unwinding angle twice that of *p*-cymene complex **1**.[5] Arene intercalation may account for the larger unwinding angle induced in DNA by **2**[5] and influence the further downstream effects of damaged DNA, for example, those involved in repair processes. Indeed repair DNA synthesis by repair-proficient HeLa cell-free extracts and nucleotide excision repair by rodent excinuclease are much less efficient when the complex contains a potentially intercalating arene compared to *p*-cymene.[29] Even though complex **1** cannot act as a DNA intercalator, it can still cause significant distortions and thermal destablisation of DNA,[5] which may explain why the IC_{50} values of complexes **1** and **2** are similar. Model complexes with guanine derivatives suggest[6] that the non-coordinated phenyl ring of [(η^6-biphenyl)-Ru(en)]$^{2+}$ adducts of DNA can undergo π–π stacking interactions with the purine ring of G, which should allow favourable intercalation into duplex DNA. In the present study we sought evidence for this in our studies of the ruthenation of the self-complementary 6-mer d(CGGCCG). HPLC and ESI-MS studies allowed us to separate and characterise mono-, di- and triruthenated adducts and the specific binding sites were identified by two-dimensional NMR spectroscopic studies. Although all three G's were readily ruthenated at N7 in the single-stranded 6-mer, only G3 and G6, and not G2, in the duplex were ruthenated, attributable to unfavourable steric interactions between the duplex and arene for binding at G2. The NMR shift changes were indicative of the intercalation of the biphenyl ring of **2**, selectively between G3 and C4 and between G6 and C5 with weakening of the GO6···NH(en) hydrogen bonding compared to adducts of **1**. Further work is in progress in our laboratory[34] on a non-self-complementary 14-mer DNA duplex with the aim of defining more fully the structural changes induced by intercalating arenes so that models of the complexes can be proposed.

Experimental Section

Materials: [(η^6-*p*-cymene)RuCl(en)]PF_6 (**1**), [(η^6-biphenyl)RuCl(en)]PF_6 (**2**) and ^{15}N-labelled **1** (^{15}N-**1**) and **2** (^{15}N-**2**) were synthesised as described previously.[1,7] The sodium salt of FPLC-purified d(CGGCCG) **I** was purchased from Oswel (Southampton, UK) and further purified by HPLC. Sodium perchlorate and acetonitrile (HPLC grade) were obtained from Fisher, and triethylammonium acetate buffer (TEAA) from Fluka.

High-performance liquid chromatography (HPLC): A Hewlett–Packard Series 1100 quaternary pump and a Rheodyne sample injector with 100 μL and 500 μL loops, a HP 1100 series UV/Vis detector and HP 1100 series Chemstation with a HP enhanced integrator were used. Analytical separations for reaction mixtures of ruthenium complexes with DNA were carried out on an ACE300–5C8 reversed-phase column (250 × 4.6 mm, 300 Å, 5 μm, Hichrom Ltd), and semipreparative work on an ACE300–5C8 reversed-phase column (250 × 10 mm, 5 μm, Hichrom Ltd) with detection at 260 nm. Mobile phases were A: 20 mM TEAA (in water, purified using a Millipore Elix 5 system) and B: 20 mM TEAA in acetonitrile. For analytical assays, the flow rate was 1.0 mL min^{-1}, for semipreparative work, 5 mL min^{-1}. A 35 min linear gradient from 2.0–16.8 % B was applied for all reaction mixtures of complex **1**. A 28 min linear gradient from 2.0–24.3 % B was applied for all reaction mixtures of complex **2**.

HPLC-electrospray ionisation mass spectrometry (HPLC-ESI-MS): Negative-ion ESI mass spectra were obtained with a Platform II mass spectrometer (Micromass, Manchester, U.K.) interfaced with a Waters 2690 HPLC system. The gradient described above was applied to an analytical ACE-5 column with a flow rate of 1.0 mL min^{-1} and a splitting ratio of 1/6. The spray voltage and the cone voltages were 3.50 kV and 40 V, respectively. The capillary temperature was 413 K with a 450 L h^{-1} flow of nitrogen drying gas. The quadrupole analyser, operated at a background pressure of 2×10^{-5} Torr, was scanned at 950 Da s^{-1}. Data were collected and analysed on a Mass Lynx (ver. 2.3) Windows NT PC data system using the Max Ent Electrospray software algorithm and calibrated versus an NaI calibration file.

NMR spectroscopy: NMR data were acquired on 800 MHz or 600 MHz Bruker Avance NMR spectrometers equipped with a triple resonance TXI (^{1}H,^{13}C,^{15}N) *xyz*-gradient probe and a triple resonance TXI (^{1}H,^{13}C,^{15}N) *z*-gradient cryoprobe, respectively. Experiments were carried out at 283 K by using dioxane as the internal reference ($\delta(^1H) = 3.767$, 298 K). NMR spectra for samples of ^{15}N-**1**, ^{15}N-**2**, **I**, **II** and the reaction mixtures of ^{15}N-**1** or ^{15}N-**2** with **I** or **II** were recorded as follows. One-dimensional ^{1}H NMR spectra were acquired typically with 256 or 1 k transients into 16 k data points over a spectral width of 20 ppm by using the double-pulsed-field-gradient-spin-echo (DPFGSE) pulse sequence.[35] Two-dimensional ^{15}N-decoupled [^{1}H,^{15}N] HSQC NMR data sets were acquired and processed according to previously reported methods.[7] Two-dimensional ^{15}N-decoupled [^{1}H,^{1}H] NOESY NMR data sets were acquired typically with 64 to 544 transients over a ^{1}H spectral width of 20 ppm into 4096 data points for each of 512 t_1 increments (States-TPPI) using mixing times of 100, 150, 250 or 400 ms. Two-dimensional ^{15}N-decoupled [^{1}H,^{1}H] COSY NMR data sets were acquired with 128 transients for each of 512 t_1 (QF) increments over a spectral width of 10 ppm. Two-dimensional ^{15}N-decoupled [^{1}H,^{1}H] TOCSY NMR data sets were acquired typically with 64 to 320 transients over a ^{1}H spectral width of 10 ppm into 4096 data points for each of 512 t_1 increments (States-TPPI) using a mixing time of 80 ms. Two-dimensional ^{15}N-decoupled [^{1}H,^{1}H] ROESY NMR data sets were acquired with 72 transients over a ^{1}H spectral width of 20 ppm into 4096 data points for each of 512 t_1 increments (States-TPPI) using a mixing time of 150 ms or 200 ms. Two-dimensional ^{15}N-edited TOCSY NMR data sets were acquired with 128 transients over a ^{1}H spectral width of 10 ppm in F2 domain and 5 ppm in F1 domain into 2048 data points for each of 128 t_1 increments (States-TPPI) using a mixing time of 80 ms. Two-dimensional ^{15}N-edited NOESY NMR data sets were acquired with 256 transients over a ^{1}H spectrum width of 20 ppm in F2 domain and 5 ppm in F1 domain into 4096 data points for each of 128 t_1 increments (States-TPPI) using a mixing time of 400 ms. The water peak in NOESY, TOCSY and ROESY experiments was suppressed by using a DPFGSE routine.[35] Water suppression for COSY experiments was achieved using a water presaturation. In all cases the ^{15}N transmitter was centred at −30 ppm and ^{15}N chemical shifts were referenced relative to $^{15}NH_4Cl$ (0 ppm). All NMR data were processed using

Xwin-nmr (Version 3.5, Bruker BioSpin Ltd). Data were processed using standard apodizing functions prior to Fourier transformation.

pH measurements: All pH measurements were made using a Corning 240 pH meter equipped with an Aldrich micro combination electrode calibrated with Aldrich standard buffer solutions of pH 4, 7 and 10. For NMR samples in 90% H_2O/10% D_2O, no correction was applied for the effect of deuterium on the glass electrode.

HPLC purification of d(CGGCCG) I: The self-complementary 6-mer DNA oligonucleotide **I** was purified on an ACE-5 reverse phase column (250×10 mm) with a gradient (B%) of 4.2–6.2% over 15 min and a flow rate of 5 mL min^{-1}. The single-strand DNA had a retention time of 4.1 min, and the fraction was identified by LC-MS (MW = 1792 Da). The solvents and TEAA were removed by freeze-drying twice, once at pH 12 and once at pH 3. The purity of **I** was checked by both HPLC and one-dimensional ^{1}H NMR spectroscopy; the concentration was determined on a Perkin Elmer Lambda 16 UV spectrometer (ε_{260} = 51.30 mM^{-1} cm^{-1}; stock solution 0.80 mM).

Preparation of duplex DNA II: D_2O (50 μL) and $NaClO_4$ (25 μL, 2 M) were added to **I** (425 μL, 0.80 mM) and the pH of the solution was adjusted to 7.0 by adding $HClO_4$ and NaOH. The final concentration of **II** was 0.34 mM (in 0.1 M $NaClO_4$). The sample was annealed by heating from 288 K to 353 K over 2 min and then cooling slowly down to 288 K over 3.5 h. The formation of **II** was monitored and confirmed by one-dimensional ^{1}H NMR spectroscopy.

Reactions of II with ^{15}N-1 and ^{15}N-2: An equimolar quantity of ^{15}N-**1** (42 μL, 4.0 mM) or ^{15}N-**2** (17 μL, 10.0 mM) was added to an NMR sample containing **II** (500 μL, 0.34 mM, 90% H_2O/10% D_2O); the final concentrations of **II** were 0.31 mM and 0.33 mM, respectively, and the pH of the solutions was adjusted to 7.00. Dioxane was added as an internal ^{1}H NMR reference. The mixtures were shaken for several minutes and kept at 298 K for three weeks (^{15}N-**1**+**II**) or 2 days (^{15}N-**2**+**II**) in the dark. The ruthenation reactions were studied by both one-dimensional ^{1}H and two-dimensional [^{1}H,^{1}H] NMR spectroscopy, and by HPLC. These mixtures were then freeze-dried and re-dissolved in 99.99% D_2O for studies of non-exchangeable protons only. Reaction mixtures (10 mL) of ^{15}N-**2** (0.34 mM) and **II** (0.34 mM) were separated on a semipreparative ACE-5 column. The fraction eluting at 14.4 min and containing **I**–Ru–G3 (Ru = [(η^6-biphenyl)Ru(en)]$^{2+}$ (**2′**)) was collected, freeze-dried, and then re-dissolved in deionised water. The resultant solution was desalted by using a Tube-O-Dialyzer (MW cut-off = 1000, Geno Technology Inc. USA). After checking the purity using an HPLC assay and measuring the concentration of DNA by UV, the aqueous solution was freeze-dried and re-dissolved in 10% D_2O/90% H_2O. Then $NaClO_4$ (25 μL, 2.0 M) was added to 500 μL of the solution, together with dioxane as internal ^{1}H NMR reference standard. The resulting ruthenated DNA solution was annealed by heating briefly from 288 K to 353 K over 2 min, followed by cooling slowly to 288 K over 3.5 h (to give duplex **II**–Ru_2–G3G9). The extent of duplex formation was verified by one-dimensional ^{1}H NMR spectroscopy, and ^{15}N-decoupled two-dimensional [^{1}H,^{1}H] TOCSY, COSY and NOESY, and two-dimensional [^{1}H,^{15}N] HSQC NMR spectra were recorded subsequently. The solution was also freeze-dried from 90% H_2O and re-dissolved in 99.99% D_2O for studies of non-exchangeable protons only.

Reactions of I with ^{15}N-1 or ^{15}N-2: Solutions of ^{15}N-**1** (150 μL, 4.0 mM) or ^{15}N-**2** (40 μL, 10.0 mM) were added into NMR tubes [containing **I** (125 μL, 0.80 mM), D_2O (50 μL) and H_2O(175 μL)], respectively; the final concentration of **I** was 0.20 mM and the ratios of Ru/**I** were 6:1 (^{15}N-**1**:**I**) or 4:1 (^{15}N-**2**:**I**); the pH of the solution was adjusted to 7.00. Dioxane was added as internal ^{1}H NMR reference. The mixtures were shaken for several minutes and kept at 310 K for two days in the dark. The reactions were investigated by HPLC and both one-dimensional ^{1}H and two-dimensional [^{1}H,^{1}H] and [^{1}H,^{15}N] NMR spectroscopy.

Acknowledgements

We thank the Wellcome Trust (Travelling Fellowship for HL and facilities in the Edinburgh Protein Interaction Centre), BBSRC (RASOR) and Oncosense Ltd for their support for this work, and Dr Haimei Chen for the gift of some of the complexes. We are grateful to Professor Malcolm Walkinshaw and Dr Paul Taylor (Institute of Structural and Molecular Biology, University of Edinburgh) for assistance with DNA crystallisation and X-ray diffraction experiments, and to colleagues in the EC COST Action D20 for stimulating discussions.

[1] R. E. Morris, R. E. Aird, P. D. Murdoch, H. M. Chen, J. Cummings, N. D. Hughes, S. Parsons, A. Parkin, G. Boyd, D. I. Jodrell, P. J. Sadler, *J. Med. Chem.* **2001**, *44*, 3616–3621.
[2] R. E. Aird, J. Cummings, A. A. Ritchie, M. Muir, R. E. Morris, H. Chen, P. J. Sadler, D. I. Jodrell, *Br. J. Cancer* **2002**, *86*, 1652–1657.
[3] K. Y. Yan, M. Melchart, A. Habtemariam, P. J. Sadler, *Chem. Commun.* **2005**, 4764–4776.
[4] M. Melchart, P. J. Sadler in *Bioorganometallics* (Ed.: G. Jaouen), Wiley-VCH, Weinheim, **2005**, pp. 39–64.
[5] O. Novakova, H. M. Chen, O. Vrana, A. Rodger, P. J. Sadler, V. Brabec, *Biochemistry* **2003**, *42*, 11544–11554.
[6] H. M. Chen, J. A. Parkinson, S. Parsons, R. A. Coxall, R. O. Gould, P. J. Sadler, *J. Am. Chem. Soc.* **2002**, *124*, 3064–3082.
[7] H. M. Chen, J. A. Parkinson, R. E. Morris, P. J. Sadler, *J. Am. Chem. Soc.* **2003**, *125*, 173–186.
[8] D. B. Zamble, S. J. Lippard, in *Cisplatin—Chemistry and Biochemistry of a Leading Anticancer Drug* (Ed.: B. Lippert), Wiley-VCH, Weinheim, **1999**, pp. 73–110.
[9] G. A. Leonard, T. W. Hambley, K. McAuleyhecht, T. Brown, W. N. Hunter, *Acta Crystallogr. Sect. D* **1993**, *49*, 458–467.
[10] Crystal trials on duplexes ruthenated with complexes **1** or **2** were carried out with sitting drops at 277 or 285 K, by using sodium cacodylate buffers (pH 4.6–7.5) containing magnesium chloride, spermine tetrahydrochloride and 2-methyl-2.4-pentanediol (MPD; 8.3–40%) equilibrated against a reservoir containing 30–100% MPD.
[11] S. L. Lam, S. C. F. AuYeung, *J. Mol. Biol.* **1997**, *266*, 745–760.
[12] J. Vinje, J. A. Parkinson, P. J. Sadler, T. Brown, E. Sletten, *Chem. Eur. J.* **2003**, *9*, 1620–1630.
[13] J. L. Beck, R. Gupta, T. Urathamakul, N. L. Williamson, M. M. Sheil, J. R. Aldrich-Wright, S. F. Ralph, *Chem. Commun.* **2003**, 626–627.
[14] J. A. Parkinson, Y. Chen, P. D. Murdoch, Z. J. Guo, S. J. Berners-Price, T. Brown, P. J. Sadler, *Chem. Eur. J.* **2000**, *6*, 3636–3644.
[15] D. R. Hare, D. E. Wemmer, S. H. Chou, G. Drobny, B. R. Reid, *J. Mol. Biol.* **1983**, *171*, 319–336.
[16] F. Y. Wang, J. Bella, J. A. Parkinson, P. J. Sadler, *J. Biol. Inorg. Chem.* **2005**, *10*, 147–155.
[17] F. Reeder, F. Gonnet, J. Kozelka, J. C. Chottard, *Chem. Eur. J.* **1996**, *2*, 1068–1076.
[18] H. Baruah, U. Bierbach, *Nucleic Acids Res.* **2003**, *31*, 4138–4146.
[19] Y. Coppel, J. F. Constant, C. Coulombeau, M. Demeunynck, J. Garcia, J. Lhomme, *Biochemistry* **1997**, *36*, 4831–4843.
[20] W. D. Wilson, Y. Li, J. M. Veal, in *Advances in DNA Sequence Specific Agents* (Ed.: L. H. Hurley), New York, **1992**, pp. 89–165.
[21] J. Lee, V. Guelev, S. Sorey, D. W. Hoffman, B. L. Iverson, *J. Am. Chem. Soc.* **2004**, *126*, 14036–14042.
[22] X. G. Liang, H. Asanuma, H. Kashida, A. Takasu, T. Sakamoto, G. Kawai, M. Komiyama, *J. Am. Chem. Soc.* **2003**, *125*, 16408–16415.
[23] H. Baruah, U. Bierbach, *J. Biol. Inorg. Chem.* **2004**, *9*, 335–344.
[24] S. H. Chou, K. H. Chin, F. M. Chen, *Proc. Natl. Acad. Sci. USA* **2002**, *99*, 6625–6630.
[25] C. Y. Lian, H. Robinson, A. H. J. Wang, *J. Am. Chem. Soc.* **1996**, *118*, 8791–8801.
[26] C. B. Nielsen, M. Petersen, E. B. Pedersen, P. E. Hansen, U. B. Christensen, *Bioconjugate Chem.* **2004**, *15*, 260–269.

[27] A. Favier, M. Blackledge, J.-P. Simorre, S. Crouzy, V. Dabouis, A. Gueiffier, D. Marion, J.-C. Debouzy, *Biochemistry*, **2001**, *40*, 8717–8726.
[28] M. J. Cocco, L. A. Hanakahi, M. D. Huber, N. Maizels, *Nucleic Acids Res.* **2003**, *31*, 2944–2951.
[29] O. Novakova, J. Kasparkova, V. Bursova, C. Hofr, M. Vojtiskova, H. M. Chen, P. J. Sadler, V. Brabec, *Chem. Biol.* **2005**, *12*, 121–129.
[30] U. M. Ohndorf, M. A. Rould, Q. He, C. O. Pabo, S. J. Lippard, *Nature* **1999**, *399*, 708–712.
[31] E. R. Jamieson, S. J. Lippard, *Chem. Rev.* **1999**, *99*, 2467–2498.
[32] F. Legendre, J.-C. Chottard, in *Cisplatin—Chemistry and Biochemistry of a Leading Anticancer Drug* (Ed.: B. Lippert), Wiley-VCH, Weinheim, **1999**, pp. 223–245.
[33] H. M. Chen, J. A. Parkinson, O. Novakova, J. Bella, F. Y. Wang, A. Dawson, R. Gould, S. Parsons, V. Brabec, P. J. Sadler, *Proc. Natl. Acad. Sci. USA* **2003**, *100*, 14623–14628.
[34] H. Liu, S. J. Berners-Price, F. Wang, J. A. Parkinson, J. Xu, J. Bella, P. J. Sadler, unpublished work.
[35] T. L. Hwang, A. J. Shaka, *J. Magn. Reson. Ser. A* **1995**, *112*, 275–279.

Received: January 24, 2006
Revised: April 12, 2006
Published online: June 28, 2006

